T-cell brain infiltration and immature antigen-presenting cells in transgenic models of Alzheimer's disease-like cerebral amyloidosis

Ferretti, M T ; Merlini, M ; Späni, C ; Gericke, C ; Schweizer, N ; Enzmann, G ; Engelhardt, B ; Kulic, L ; Suter, T ; Nitsch, R M

Abstract: Cerebral beta-amyloidosis, one of the pathological hallmarks of Alzheimer's disease (AD), elicits a well-characterised, microglia-mediated local innate immune response. In contrast, it is not clear whether cells of the adaptive immune system, in particular T-cells, react to cerebral amyloidosis in AD. Even though parenchymal T-cells have been described in post-mortem brains of AD patients, it is not known whether infiltrating T-cells are specifically recruited to the extracellular deposits of beta-amyloid, and whether they are locally activated into proliferating, effector cells upon interaction with antigen-presenting cells (APCs). To address these issues we have analysed by confocal microscopy and flow-cytometry the localisation and activation status of both T-cells and APCs in transgenic (tg) mice models of AD-like cerebral amyloidosis. Increased numbers of infiltrating T-cells were found in amyloid-burdened brain regions of tg mice, with concomitant up-regulation of endothelial adhesion molecules ICAM-1 and VCAM-1, compared to non-tg littermates. The infiltrating T-cells in tg brains did not co-localise with amyloid plaques, produced less interferon-gamma than those in controls and did not proliferate locally. Bona-fide dendritic cells were virtually absent from the brain parenchyma of both non-tg and tg mice, and APCs from tg brains showed an immature phenotype, with accumulation of MHC-II in intracellular compartments. These results indicate that cerebral amyloidosis promotes T-cell infiltration but interferes with local antigen presentation and T-cell activation. The inability of the brain immune surveillance to orchestrate a protective immune response to amyloid-beta peptide might contribute to the accumulation of amyloid in the progression of the disease.

DOI: https://doi.org/10.1016/j.bbi.2016.02.009

DOI: https://doi.org/10.1016/j.bbi.2016.02.009

Brain, Behavior, and Immunity 54 (2016) 211–225

Contents lists available at ScienceDirect

Brain, Behavior, and Immunity

journal homepage: www.elsevier.com/locate/ybrbi

Full-length Article

T-cell brain infiltration and immature antigen-presenting cells in transgenic models of Alzheimer's disease-like cerebral amyloidosis

M.T. Ferretti [a,*], M. Merlini [a], C. Späni [a], C. Gericke [a], N. Schweizer [b], G. Enzmann [c], B. Engelhardt [c], L. Kulic [a], T. Suter [b], R.M. Nitsch [a]

[a] Institute for Regenerative Medicine (IREM), University of Zurich, Schlieren, Wagistrasse 12, 8952, Switzerland
[b] Neurology, Neuroimmunology and Multiple Sclerosis Research, University Hospital Zurich, Sternwartstrasse 14, 8006 Zurich, Switzerland
[c] Theodor Kocher Institute, University of Bern, Freiestrasse 1, 3012 Bern, Switzerland

ARTICLE INFO

Article history:
Received 2 December 2015
Received in revised form 26 January 2016
Accepted 9 February 2016
Available online 9 February 2016

Keywords:
Alzheimer's disease
Amyloid-beta peptide
MHC-II
T-cell
Interferon gamma

ABSTRACT

Cerebral beta-amyloidosis, one of the pathological hallmarks of Alzheimer's disease (AD), elicits a well-characterised, microglia-mediated local innate immune response. In contrast, it is not clear whether cells of the adaptive immune system, in particular T-cells, react to cerebral amyloidosis in AD. Even though parenchymal T-cells have been described in *post-mortem* brains of AD patients, it is not known whether infiltrating T-cells are specifically recruited to the extracellular deposits of beta-amyloid, and whether they are locally activated into proliferating, effector cells upon interaction with antigen-presenting cells (APCs). To address these issues we have analysed by confocal microscopy and flow-cytometry the localisation and activation status of both T-cells and APCs in transgenic (tg) mice models of AD-like cerebral amyloidosis. Increased numbers of infiltrating T-cells were found in amyloid-burdened brain regions of tg mice, with concomitant up-regulation of endothelial adhesion molecules ICAM-1 and VCAM-1, compared to non-tg littermates. The infiltrating T-cells in tg brains did not co-localise with amyloid plaques, produced less interferon-gamma than those in controls and did not proliferate locally. *Bona-fide* dendritic cells were virtually absent from the brain parenchyma of both non-tg and tg mice, and APCs from tg brains showed an immature phenotype, with accumulation of MHC-II in intracellular compartments. These results indicate that cerebral amyloidosis promotes T-cell infiltration but interferes with local antigen presentation and T-cell activation. The inability of the brain immune surveillance to orchestrate a protective immune response to amyloid-beta peptide might contribute to the accumulation of amyloid in the progression of the disease.

1. Introduction

T-cells constantly patrol body tissues as part of the physiological process of immune surveillance (von Andrian and Mackay, 2000). Upon recognition of their cognate antigen exposed on mature antigen-presenting cells (APCs), T-cells undergo activation, proliferate and exert effector functions, such as cytotoxicity in the case of $CD8^+$ T-cells and activation of macrophages and antibody-producing B cells in the case of $CD4^+$ T-helper cells. In the CNS, physiological immune surveillance is mediated by patrolling T-cells and mature APCs found in the perivascular and meningeal spaces, and at the blood–cerebrospinal fluid (CSF) barrier of the choroid plexus (CP) (Ransohoff et al., 2003; Ousman and Kubes, 2012).

In contrast to CSF-associated patrolling T-cells, T-cells retained in the brain parenchyma often reflect an on-going pathology. In autoimmune conditions such as multiple sclerosis, autoreactive T-cells play a causative role in fostering macrophage-mediated demyelination (Ciccarelli et al., 2014). In Alzheimer's disease (AD)-related neurodegeneration, characterised by the accumulation of intracellular aggregates of abnormally phosphorylated tau and extracellular deposition of aggregated amyloid-beta peptide (Aβ) (Selkoe, 2011), the role of the immune system is less well understood (Town, 2010).

While several studies have demonstrated the presence of $CD4^+$ and $CD8^+$ T-cells in *post-mortem* brains of AD patients (Rogers et al., 1988; Togo et al., 2002; Itagaki et al., 1988), their significance is a

Abbreviations: AD, Alzheimer's disease; Aβ, amyloid-beta peptide; APCs, antigen-presenting cells; CAA, cerebral amyloid angiopathy; CP, choroid plexus; CSF, cerebrospinal fluid; DCs, dendritic cells; FI, fluorescence intensity; IFN-γ, interferon gamma; MHC-I, MHC-II, major histocompatibility class I and II; tg, transgenic.

* Corresponding author.
E-mail address: mariateresa.ferretti@bli.uzh.ch (M.T. Ferretti).

http://dx.doi.org/10.1016/j.bbi.2016.02.009
0889-1591/

matter of debate. It is not clear whether T-cells are specifically recruited to amyloid deposits in AD brains, and very little is known on their activation status. Activated IFN-γ producing-T-cells could promote macrophage and microglia receptor-mediated phagocytosis (Schroder et al., 2004), thus supporting beneficial clearance of extracellular amyloid. On the other hand, overt T-cell activation could result in direct cytotoxicity and macrophage-mediated tissue damage, thereby contributing to neuronal demise (Aloisi et al., 2000b). Hence, the activation state of the infiltrating T-cells might be disease-relevant.

To elucidate this issue we have analysed T-cell numbers, localisation and phenotype in transgenic (tg) mouse models of AD-like cerebral amyloidosis. We show that cerebral amyloidosis is associated with brain infiltration of T-cells, which do not co-localise with amyloid deposits, do not proliferate locally and display low expression of the effector cytokine IFN-γ.

2. Materials and methods

2.1. Transgenic mice

ArcAβ (Knobloch et al., 2007); APP-PS1-dE9 (Jankowsky et al., 2004); Tg2576 (Hsiao et al., 1996); E22ΔAβ (Kulic et al., 2012); recombination activating gene 2 (RAG2) knockout mice (Shinkai et al., 1992) were used. ArcAβ and APP-PS1-dE9 were on a congenic C57BL/6 background; Tg2576 were on a hybrid C57BL/6 and SJL background; E22ΔAβ were on hybrid C57BL6 and DBA/2 background. In each experiment we balanced the genders across genotypes; no gender-specific effect was noted. The mice were kept in OHB conditions, at 22 °C ± 1 °C and a 12 h light–dark cycle beginning at 7:00 AM. Water and food were available *ad libitum*. Experiments were conducted in accordance with the Swiss law for care and use of animals ("455.163 Tierversuchsverordnung" 2010) and were approved by the veterinarian authorities of the Canton of Zurich (license number 145/2014). This report adheres to the ARRIVE guidelines for animal research.

2.2. Microbiological examination

Brains from two non-tg and two tg mice (2 year-old) underwent the following microbiological examination: PCR for Lymphocytic choriomeningitis, Theiler's encephalomyelitis and mouse hepatitis viruses; bacteriology culture (performed by MicroBioS GmbH, Reinach, Switzerland).

2.3. Flow-cytometry analyses

Sacrifice and mononuclear cell-suspension preparation – Mice were sacrificed via isoflurane inhalation and quickly perfused with Ringer solution (Braun Medical, Emmenbruecke, Switzerland). After removal of meningi, brain regions of interest were dissected on ice. Lateral, third and fourth ventricle-choroid plexus were used. Mononuclear single cell suspension was prepared according to standard protocols (Suter et al., 2003). For cerebrum (whole brain without cerebellum and choroid plexus), minced samples were digested for 1 h at 37 °C in HBSS containing 50 μg/ml DNase I and 100 μg/ml collagenase/dispase (Roche, Rotkreuz, Switzerland). The suspension was passed through a 100 μm Nylon mesh (Falcon, BD Biosciences, Bedford, MA, USA), pelleted, resuspended in 30% Percoll (Amersham, GE Healthcare, Uppsala Sweden) in HBSS and centrifuged at 15,500 rpm for 30 min at 4 °C. After eliminating the myelin debris via aspiration, the mononuclear cell phase was collected. Choroid plexus samples were enzymatically digested at 37 °C for 30 min, passed through a 100 μm mesh, washed and used directly. Spleens were minced in RPMI plus 5% FCS, digested with 100 μg/ml collagenase–dispase and 50 μg/ml DNaseI for 20 min at RT, passed through a 100 μm Nylon mesh, processed with ACK lysis buffer, washed in HBSS and used for staining. *Surface staining* – CNS-mononuclear cells and splenocytes were washed in FACS buffer (HBSS, 2% FCS, 10 mM EDTA, 0.01% NaN_3). After treatment with an antibody against Fc receptor (anti-mouse CD16/32, TrueStain FcX TM, BioLegend, san Diego, CA, USA), the cells were stained for 15 min at 4 °C with specific antibodies, washed and analysed. *Intracellular staining* – Intracellular stainings were performed with the eBioscience kit (n.72-5775, San Diego, CA, USA) according to manufacturer's instructions. *DC panels* – In each experiment we included at least eight non-tg and eight tg mice. For the ArcAβ 24-month-old experiment, a total of nine non-tg and ten ArcAβ APP-tg animal were used; we analysed the cerebrum from nine tg and seven non-tg mice. Choroid plexuses were removed from nine non-tg and ten tg animals. They were pooled (two-four/sample), yielding a final $n = 3$ of bulk samples/genotype. The spleens were dissected from four non-tg and four tg animals. A multicolour FACS study was performed with a BD LSR Fortessa analyzer. The panel for surface markers was: BV605-CD11c; FITC-MHCII; PE-CY5-B220; PE-CY5.5-CD45; PE-CY7-CD11b; PE-TR-CD80; APC-Cy7-CD86; APC-CD4; Alexa700-CD8a (all from eBioscience, San Diego, CA, USA). In some experiments, PE-CD11c, FITC-MHC-I and PE-MHC-II were used (from eBioscience, San Diego, CA, USA). The panel for intracellular staining was: FITC-MHCII; PE-CD11c; PE-CY5.5-CD45; APC-CD11b (all from eBioscience, San Diego, CA, USA). A fixable live-dead dye to exclude dead cells (Molecular Probes, Eugen, OR, USA) and compensation beads to set the compensation matrix (eBioscience, San Diego, CA, USA) were used. In some experiments, quantification beads were used (AccuChek Counting beads, Life Technologies, Invitrogen Corporation, MD, USA). Negative controls included isotype controls and fluorescence-minus-one stainings. Splenocytes were used as biological positive controls. *T-cell panel* – For 20-month-old ArcAβ mice, we analysed six non-tg and seven tg mice. Whole brains and splenocytes from each mouse were stained for both surface and intracellular markers. For cytokine detection, the cells were re-stimulated *in vitro* at 37 °C with PMA (10^{-7} M) and ionomycin (1 μg/ml) in the presence of GolgiPlug (BD Bioscience, Bedford, MA, USA). The panel used was: Surface: PE-CD45, Alexa700-CD8 (eBioscience, San Diego, CA, USA), APC-Cy7.7-CD4 (from BioLegend, San Diego, CA, USA); intracellular: PE-CY5-FoxP3, Pacific-Blue-IFNγ, APC-IL10 (eBioscience, San Diego, CA, USA), PE.CY7-IL17A (from BioLegend, San Diego, CA, USA), TNFα-FITC (eBioscience, San Diego, CA, USA), Ki67-PE-TR (BioLegend, San Diego, CA, USA). Live-dead dye and compensation beads were used (see above). Counting beads (AccuChek Counting beads, Life Technologies, Invitrogen Corporation, MD, USA) were added to CNS samples. Five millions splenocytes were stained from each animal (measured via Neubauer chamber and Coulter counter). Controls included unstained CNS samples and single stained splenocytes. All samples were acquired and analysed blinded to genotype. *Definitions of cells of the myeloid lineage* – Microglia were defined as $CD45^{int}CD11b^{+}$ cells, while $CD45^{hi}CD11b^{+}$ cells were considered as periphery-derived CNS myeloid cells ("myeloid cells"). Conventional myeloid DCs (cDCs) were defined as $CD45^{+}CD11c^{+}CD11b^{+}MHC\text{-}II^{+}$, as previously published (Hesske et al., 2010) and in accordance with a recently proposed classification (Guilliams et al., 2014).

2.4. Bright-field immunohistochemistry

CD3, CD4, CD8, MHC-II – Mice were anesthetised via ketamine–xylazine injection (10 ml/g bw) and quickly perfused with PBS. The brains were dissected on ice and fixed in 4% paraformaldehyde (granular, n.19210 Electron Microscopy Science) for 24 h (or 6 h for detection of CD4 and CD8) and cryoprotected in 30% sucrose.

Free-floating, 40 μm-thick sections were blocked with 10% donkey and goat sera O/N, followed by treatment with avidin biotin blocking kit (Vectorlabs, SP2001, Burlingame, CA, USA). The primary antibodies were incubated O/N at 4 °C followed by 1 h incubation with 1:200 biotinylated secondary antibody in 10% sera. The ABC kit (Vector, PK6100 Standard, Burlingame, CA, USA) was used according to manufacturer's instructions. The staining was revealed using nickel-enhanced DAB (n.1855910, Thermo Fisher, Rockford, IL, USA). Haematoxylin counterstaining was performed using Mayer's hemalum solution (T865, Roth GmbH, Karlsruhe, Germany). Negative controls included omission of primary antibody and RAG2ko mouse model. Positive controls were spleen and liver tissue. *VCAM1–ICAM1* – Mice were anesthetised via ketamine–xylazine injection (10 ml/g bw) and perfused with 1% paraformaldehyde in PBS, pH 7.4; their brains removed, embedded in Jung tissue freezing medium (Leica Microsystems, Nussloch, Germany) and frozen in a dry ice/isopentane bath. Cryostat sections (6 μm) were fixed in −20° C acetone and stained using a three-step immunoperoxidase staining kit (Vector).

2.5. Quantification $CD3^+$ T-cell density

Per each animal, two whole sections corresponding to bregma −0.70 (for cortical density) and three sections corresponding to bregma −0.70, −1.94, −3.16 (for total density) were stained with anti-CD3 antibody as described above. Bright-field microscopy images were acquired using a Leica DM4000B microscope (Leica, Wetzlar, Germany) equipped with an Olympus DP71 digital camera (Olympus, Volketswil, Switzerland). The number of $CD3^+$ T-cells was quantified in live mode using the meander tool of the newCAST module of the Visiopharm software (Visiopharm, HØrsholm, Denmark). For measurement of total $CD3^+$ density, a region of interest (ROI) was drawn around each section. For cortical measurements, a ROI including somatosensory (S1BF, S1FL and S1HL regions), motor cortex 1 and 2 and cingulate cortex was drawn (see also Supplementary Fig. 1B). The automatic stage was set to randomly move within the ROI, sampling 50% of the ROI area. On average, 15 images were quantified per ROI. $CD3^+$ T-cells were counted by the experimenter blind to the origin of the samples; the numbers of counted elements and ROI size were automatically recorded by the software. Counts were normalised to the size of the respective ROI/2 and densities averaged across the sections yielding one value per animal. All samples were acquired and analysed blinded to genotype.

2.6. Prussian Blue staining and quantification

Prussian Blue staining was performed on CD3-stained sections (3/animal, corresponding to bregma −0.70, −1.94, −3.16) by incubation with 1:1 solution of HCl 2% and 2% potassium ferrocyanide trihydrate ($K_4[Fe(CN)]_6{\cdot}3H_2O$, Sigma-Aldrich, St Louis, MO, USA) in distilled water. Images were acquired using a Leica DM4000B microscope (Leica, Wetzlar, Germany) equipped with an Olympus DP71 digital camera (Olympus, Volketswil, Switzerland). The number of $CD3^+$ T-cells and Prussian Blue deposits was quantified in live mode using the meander tool of the newCAST module of the Visiopharm software (Visiopharm, Hørsholm, Denmark). A region of interest (ROI) was drawn around each section. The automatic stage was set to randomly move within the ROI, sampling 50% of the ROI area. On average, 15 images were quantified per ROI. Total $CD3^+$ T-cells, total Prussian Blue deposits and Prussian Blue – associated-$CD3^+$ T-cells (either directly contacting the microhaemorrhage or within a radius of 10 μm from it) were counted in each image by the experimenter blind to the origin of the samples. Numbers of counted elements and ROI size were automatically recorded by the software. Counts were normalised to the size of the respective ROI/2 and densities averaged across the three sections yielding one value per animal. All samples were acquired and analysed blinded to genotype.

2.7. Immunofluorescence on mouse tissue

The free-floating sections were blocked for 1 h at RT in 10% sera and incubated O/N with the proper primary antibody. The next day the sections were incubated with the appropriate secondary antibody for 2 h. Sudan Black B (#199664, Sigma-Aldrich, St Louis, MO, USA; 0.1% solution in 70% ethanol) was applied to eliminate lipofuscin autofluorescence. DAPI was used as counterstaining agent.

2.8. Thioflavin staining

The sections were treated with Thioflavin S (0.1% solution in 50% ethanol, T1892, Sigma-Aldrich, St Louis, MO, USA) for 5 min.

2.9. Extravasation study, correlation $CD3^+$ T-cells-amyloid fractional area and amyloid-$CD3^+$ T-cell association study

Eight tg and seven non-tg ArcAβ mice aged 15 months were sacrificed via isoflurane inhalation. Non-perfused brains were fixed in 4% paraformaldehyde for 12 h and cryoprotected in 30% sucrose for 30 h. Hundred micrometre-thick free-floating sections were washed in Trizma-buffered saline containing 0.2% Triton X-100 (TBS-T, pH 7.4), treated with proteinase K antigen retrieval for 10 min at 37 °C, followed by immuno-blocking in 10% donkey serum in TBS-T for 1 h at RT. The sections were subsequently incubated with rat anti-mouse CD3, rabbit anti-pan laminin, and mouse anti-Aβ antibody for 48 h at 4 °C, followed by washing in TBS-T and incubation in fluorescently tagged secondary antibodies (donkey anti-rat-Cy3, donkey anti-rabbit-FITC, and donkey anti-mouse-Cy5, Jackson Immunoresearch Labs, West Grove, PA, USA) for 24 h at 4 °C. Confocal microscopy images were acquired from the cortex (forelimb and barrel field somatosensory region, cingulate cortex 1 and 2, and the primary visual cortex), hippocampus (granular layer of the dentate gyrus and the *cornu ammonis* 1, 2, and 3), and the corpus callosum of each mouse brain using a Leica SP8 confocal microscope fitted with a 20× objective (Leica, Wetzlar, Germany) (see also Supplementary Fig. 1B for sampling). The acquired images of each mouse were combined in Z-projected image stacks in the ImageJ imaging software (National Institutes of Health, Bethesda, ML, USA). All samples were acquired and analysed blinded to genotype. *Quantification of infiltrating versus intravascular T-cells*: Total, infiltrating and intravascular $CD3^+$ T-cells were counted in the entire Z-stack (80 μm) and normalised to the vessel density (μm^3) in each brain section. *Correlation infiltrating T-cells-amyloid fractional area:* The number of extravasated $CD3^+$ T-cells and the area covered by 6E10-positive Aβ plaques was quantified using a semi-automatic Matlab script generated in-house. The Aβ/6E10-Cy5 and CD3-Cy3 confocal image stacks were maximum-projected, converted to an 8-bits (grey-scale) format and thresholded. The number of CD3- and Aβ/6E10-positive hits was calculated by implementing Matlab's "regionprops" tool code in the script. $CD3^+$ T-cells were calculated as counts and the Aβ/6E10-positive hits as fractions of the total image size. *Quantification of amyloid β and non-amyloid β-associated infiltrating $CD3^+$ T-cells*: Quantification of infiltrating non-Aβ-, parenchymal Aβ plaque- and CAA-associated $CD3^+$ T-cells was performed on confocal z-stack images of 100-μm thick mouse brain sections stained for pan-laminin, CD3 and Aβ. Areas with xyz dimensions of 1 mm × 1 mm × 100 μm were quantified within the brain areas of interest. $CD3^+$ T-cells within a 10-μm perimeter around the outer edge of a parenchymal Aβ plaque or vascular Aβ were consid-

ered Aβ plaque- and CAA-associated, respectively. $CD3^+$ T-cells that did not fulfil these spatial distribution criteria were considered non-Aβ-associated.

2.10. Antibodies immunohistochemistry

For the detection of CD3 we used the clone KT3 (rat anti-mouse, MCA 500GA, AbD Serotec, Kidlington, UK) and 145-2C11 from BD Bioscience (Armenian-hamster anti-mouse CD3, #553058, Bedford, MA, USA). Anti-CD4 and CD8 antibodies were from BD Bioscience (rat anti-mouse CD4, clone GK1.5, #553727 and rat anti-mouse CD8, clone 53-6.7, #553027, Bedford, MA, USA). Rabbit anti-mouse pan laminin was from Sigma-Aldrich (L9393, St Louis, MO, USA). For vascular adhesion molecules the primary antibodies employed were: rat anti-mouse VCAM1 (clone 2A11.12), rat anti-mouse ICAM1 (clone 25ZC7), rat anti human CD44 (clone 9B5) was used as IgG control (Enzmann et al., 2013). For MHC-II detection we used the purified 2G9 clone from BD Bioscience (rat anti-mouse class I-A/I-E, #553621, Bedford, MA, USA). The clone SP6 (RM-9106-S0, Thermo Fisher, Rockford, IL, USA) was used to detect Ki67. For detection of MHC-I we used a rat anti-mouse antibody from BMA biomedicals (T2105, Augst, Switzerland). Biotinylated goat anti-mouse, – rabbit, and -Armenian hamster and donkey anti-mouse, -rabbit, -guinea-pig or -rat conjugated with Cy3 or DyeLight were from Jackson Immunoresearch Labs (West Grove, PA, USA).

2.11. Statistical analysis

Data are presented as the mean ± S.E.M. Statistical analysis was performed using the GraphPad Prism software (LaJolla, CA, USA). Two-group comparisons were performed using two-tailed Student's *t*-test; Welsh's correction was used in case of unequal variances. Multiple-group comparisons were performed with ANOVA or 2-way-ANOVA, using the Bonferroni post-hoc test. Alpha level to determine significance was set at $p < 0.05$.

3. Results

3.1. Increased $CD3^+$ T-cell occurrence in ArcAβ mouse brains compared to non-tg littermates

In order to study the effect of cerebral amyloidosis on T-cell infiltration of brain, we have assessed the occurrence of $CD3^+$ T-cells via immunohistochemistry in 12- and 22–24-month-old ArcAβ mice as compared to age-matched, non-tg littermates.

$CD3^+$ T-cells were only rarely observed in non-tg mice younger than 11 month-old, mostly localised at expected sites of immune surveillance such as the CP stroma and the meninges (data not shown). In contrast, aged (12- and in 22–24-month-old) non-tg mice consistently displayed $CD3^+$ T-cell invasion in periventricular areas, in white matter bundles (such as the corpus callosum, internal and external capsulae, fimbria and fornix) and in the rostro-migratorial stream (Fig. 1A). The grey matter of aged non-tg mice was largely devoid of T-cells, with the exception of small number of cells in striatum and hippocampus. Quantification of $CD3^+$ T-cells revealed significantly increased total $CD3^+$ T-cell density in brains from 22–24-compared to 12-month-old non-tg mice (Fig. 1C).

As opposed to age-matched non-tg littermates, several $CD3^+$ T-cells were present throughout the grey matter of cerebral cortex of aged ArcAβ mice (Fig. 1B). The $CD3^+$ T-cells appeared both clustered and dispersed in the neuropil, with $CD8^+$ being the predominant T-cell subtype. Both the total (i.e. measured in white and grey matter from the whole brain section) and the cortical (i.e. measured exclusively in grey matter of cerebral cortex) densities of brain $CD3^+$ T-cells were found to be significantly up-regulated at 22–24-months of age in ArcAβ mice compared to non-tg controls (Fig. 1C and D). At 12-months of age only the cortical $CD3^+$ T-cell density was increased in ArcAβ mice compared to littermate controls, suggesting a local redistribution of the cells (Fig. 1E).

Flow-cytometry analysis of *ex vivo* isolated mononuclear cells derived from whole brains (thus combining grey matter- and white matter-associated cells) revealed that $CD8^+$ but not $CD4^+$ T-cell numbers were increased in ArcAβ mice, reaching significance at the 24-month-old time-point (Fig. 1E). Importantly, no significant difference in splenic T-cell counts was found between non-tg and ArcAβ mice. Hence, compared to non-tg controls, ArcAβ mice harbour increased cerebral $CD3^+CD8^+$ T-cells, which are focally accumulated in grey matter areas at 12-months of age and become wide-spread at 22–24-months of age.

3.2. $CD3^+$ T-cells infiltrate the brain parenchyma of ArcAβ mice

To determine whether the $CD3^+$ T-cells observed in ArcAβ mouse brains had migrated into the parenchyma or whether they were trapped in the perivascular space, 100-μm-thick brain sections from non-perfused 15-month-old ArcAβ and non-tg littermates were double-labelled for CD3 and pan-laminin, followed by confocal imaging and 3D reconstruction (Fig. 2A). This allowed us to quantify in each section both infiltrating (i.e. beyond the pan-laminin layer, such as cells 2–3 in Fig. 2B) and intravascular $CD3^+$ T-cells.

Compared to non-tg littermate controls, ArcAβ brains displayed significantly more infiltrating, but not intravascular, $CD3^+$ T-cells in all cortical areas examined, as well as in the hippocampal CA1 field and in the corpus callosum (Table 1). The increased numbers of infiltrating cells was not due to hyper-vascularization in ArcAβ mice, since vessel density was not significantly different between genotypes (data not shown). Hence, ArcAβ mice brains were invaded by $CD3^+$ T-cells, which had crossed the *glia limitans*, resided in the parenchyma and closely associated with CNS-resident cells such as astrocytes (GFAP staining, Fig. 2D), neurons (NeuN staining, Fig. 2E) and microglial/myeloid cells (Iba-1 staining, Fig. 2F) as revealed by confocal microscopy. Furthermore, we have observed that, on average, 77% of total cortical $CD3^+$ T-cells detected in ArcAβ cerebral cortex were infiltrating, as opposed to 35% in non-tg littermate controls (Fig. 2C), indicating a shift in the intravascular versus parenchymal T-cell pool in ArcAβ brains.

3.3. Relationship between cerebral amyloidosis and $CD3^+$ T-cells in ArcAβ mice

The increased frequency of infiltrating $CD3^+$ T-cells (Fig. 2C) suggested the presence of a T-cell attraction- and/or retention-factor in brains from ArcAβ mice. To ascertain whether cerebral beta-amyloidosis was the cause of T-cell attraction/retention, we compared the occurrence of $CD3^+$ T-cells between several, independent amyloid-depositing tg models, and the E22ΔAβ mice, which over-express amyloid precursor protein (APP) but harbour a pathology limited to intracellular Aβ and leptomeningeal amyloidosis (Kulic et al., 2012) (Fig 3A, upper panel). While $CD3^+$ T-cells infiltrated the grey matter of all amyloid-depositing mouse brains (Fig. 3A, lower panel), no $CD3^+$ T-cells were detected in the grey matter of the E22ΔAβ mice. These results suggested that extracellular, parenchymal amyloidosis is required for T-cell invasion.

To further examine this possibility, we studied the relationship between $CD3^+$ T-cells and 6E10-positive amyloid deposits in brains of 15-month-old ArcAβ mice, which are heavily burdened by amyloid pathology consisting of both cerebral amyloid angiopathy (CAA)- and parenchymal plaques. Here, we found a significant cor-

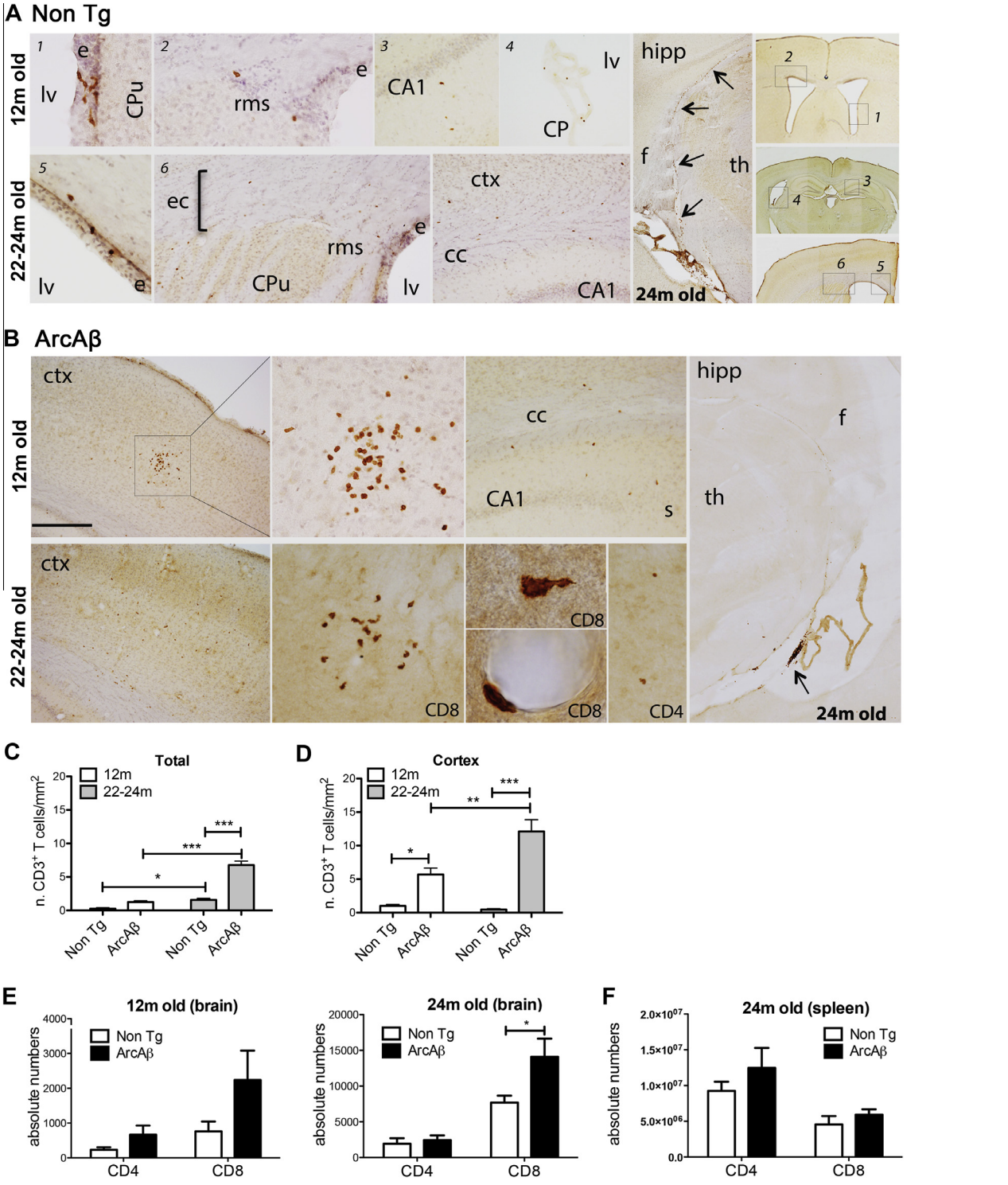

Fig. 1. Increased occurrence of $CD3^+$ T-cells in brains of aged ArcAβ mice. (A) Representative micrographs illustrating typical white-matter associated $CD3^+$ T-cell distribution observed in non-tg mice of 12- and 24-months of age (upper and lower panel, respectively). Arrows indicate $CD3^+$ T-cells lining the tissue connecting fimbria to CP. cc: corpus callosum, CP: choroid plexus, CPu: Caudatum Putamen, e: ependyma, ec: external capsula, hf: hippocampal fissure, lv: lateral ventricle, rms: rostro migratorial stream, ctx: cortex, f: fimbria, th: thalamus. (B) Representative micrographs illustrating typical grey-matter $CD3^+$ T-cell distribution in ArcAβ mice of 12- and 24-months of age (upper and lower panel, respectively; CD4 and CD8 staining are also shown). Arrow points to a cluster of $CD3^+$ T-cells in the proximity of the CP at the ventral horn of the lateral ventricles (arrow). s: subiculum, ctx: cortex. (C) Quantification of $CD3^+$ T-cell density, as detected via immunohistochemistry in whole sections from 12 and 22-month-old ArcAβ mice and non-tg littermate controls ($n = 5–6$ per group, $^*p < 0.05$, $^{***}p < 0.001$, 2-way-ANOVA followed by Bonferroni post-hoc test; effect of age, genotype and interaction: $p < 0.001$). (D) Quantification of $CD3^+$ T-cell density, as detected via immunohistochemistry in grey matter of cerebral cortex (see Supplementary Fig. 1B for exact sampling area) from 12- and 22-month-old ArcAβ mice and non-tg littermate controls ($n = 5–6$ per group; $^*p < 0.05$, $^{**}p < 0.01$, $^{***}p < 0.001$, 2-way-ANOVA followed by Bonferroni post-hoc test; effect of age: $p < 0.01$, effect of genotype: $p < 0.001$, interaction: $p < 0.01$). (E) Quantification of absolute numbers of lymphocytes via multicolour flow-cytometry analysis of brain-derived mononuclear cell suspensions from 12- and 24-month-old ArcAβ and non-tg littermate controls ($n = 6–8$ per group, $^*p < 0.05$, Student's t-test). (F) Quantification of absolute numbers of lymphocytes via multicolour flow-cytometry in spleen-derived mononuclear cell suspensions from 24-month-old ArcAβ and non-tg littermate controls.

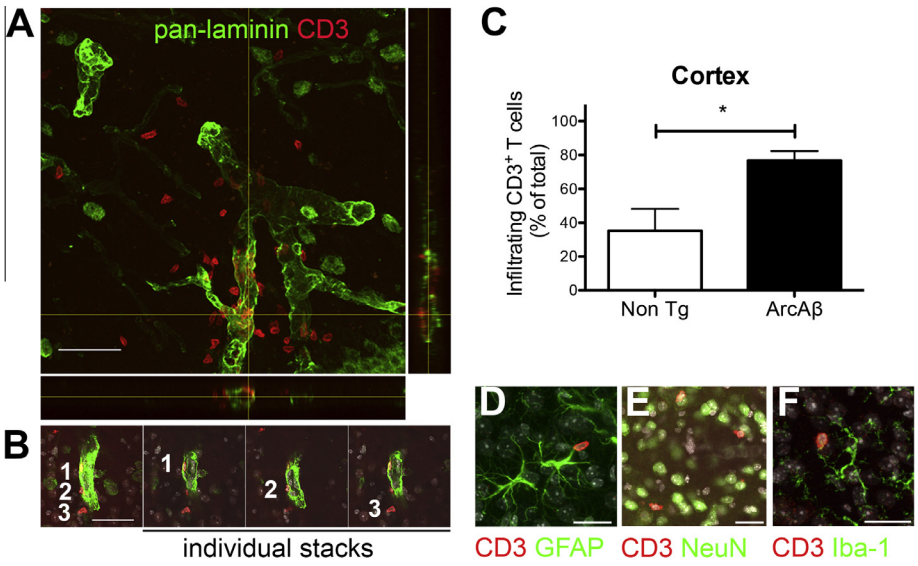

Fig. 2. T-cells infiltrate the brain parenchyma of ArcAβ mice. (A) Z-stack maximal projection of a representative pan-laminin/CD3 double labelling on non-perfused 15-month-old ArcAβ mouse brain. Scale bar: 50 μm. (B) Z-stack maximal projection and three individual stacks of a pan-laminin/CD3 double labelling on an ArcAβ mouse brain. Examples of perivascular (1), juxtavascular (2) and parenchymal (3) T-cells are shown. Scale bar: 20 μm. (C) Quantification of infiltrated $CD3^+$ T-cells from brains of non-perfused 15-month-old ArcAβ mice ($n = 8$) and non-tg littermate controls ($n = 7$) in somatosensory and cingulate cortex. Data are expressed as percentage over total number of $CD3^+$ T-cells. ($^*p < 0.05$, Student's t-test). (D–F) Representative micrographs illustrating the relationship between $CD3^+$ T-cells and astrocytes (GFAP staining, D), neurons (NeuN staining, E) and microglial cells (Iba-1 staining, F) in cerebral cortex of aged ArcAβ mice. Z-stack maximal projections images are shown. Scale bars: 20 μm.

Table 1
Quantification of intravascular and infiltrated $CD3^+$ T-cells in brains of 15-month-old ArcAβ mice ($n = 8$) and non-tg littermates ($n = 7$).

Brain area	Intravascular $CD3^+$ T-cells (n/field ± S.E.M.)		Infiltrating $CD3^+$ T-cells (n/field ± S.E.M.)	
	Non-tg	ArcAβ	Non-tg	ArcAβ
GrDG	2.57 ± 0.81	1.63 ± 0.56	4.71 ± 1.21	12 ± 4.78
CA1	1.83 ± 0.69	2.13 ± 0.93	2.83 ± 0.61	9.25 ± 2.30**
CA2, CA3	2.830.81	1 ± 0.38	4.17 ± 0.94	5.38 ± 1.19
Corp call	5.86 ± 1.68	4.63 ± 1.25	6 ± 2.27	32 ± 9.06**
S1FL	0.71 ± 0.36	2.130.55	0.57 ± 0.30	11.88 ± 4.02**
S1BF	0.67 ± 0.46	1.75 ± 1.02	0.17 ± 0.15	16.5 ± 5.79**
Cg1, Cg2	3.14 ± 1.56	2.880.46	1.290.75	7.13 ± 2.33**
V1	0.33 ± 0.20	1 ± 0.33	0.67 ± 0.20	8.75 ± 3.93*

GrDG = granular layer of the dentate gyrus, CA1, 2, and 3 = corpus ammonis 1, 2, and 3, resp., Corp call = corpus callosum, S1FL = somatosensory cortex, front leg, S1BF = somatosensory cortex, barrel field, Cg1, Cg2 = cingulate cortex 1 and 2, V1 = visual cortex 1.
$^*p < 0.05$; $^{**}p < 0.01$, Mann–Whitney t-test (compared to non-tg).

relation between $CD3^+$ T-cell counts and the fractional amyloid area (including both parenchymal plaques and CAA) in cerebral cortex and hippocampus. (Fig. 3B, $p < 0.01$, Pearson's correlation analysis). However, microscopic examination revealed that only 34% of the total $CD3^+$ T-cells detected were spatially associated with Aβ, and of these Aβ-associated cells, the majority (70%) accompanied CAA rather than parenchymal plaques (Fig. 3C–E). Taken together, these data suggest that extracellular amyloid deposition promotes T-cell infiltration; however, the effect is likely to be indirect since $CD3^+$ T-cells are not consistently associated with amyloid deposits.

3.4. Possible mechanisms of $CD3^+$ T-cell brain infiltration

We next sought to elucidate the mechanism of $CD3^+$ T-cell infiltration in ArcAβ mice brains. Since T-cells occasionally decorated Aβ-laden vessels, we reasoned that microhemorrhages, which often accompany CAA, could be the cause of T-cell invasion. The spatial association between $CD3^+$ T-cells and Prussian Blue (PB)-positive microhemorrhages was examined in brains from 12- and 22-month-old ArcAβ via immunohistochemistry. PB-associated $CD3^+$ T-cells were only occasionally observed in 12-month-old tg mice (in 1 out of 5 mice), while they were consistently found in 22-month-old mice (in 4 out of 5 mice, Fig. 4A lower panel). However, the PB-associated $CD3^+$ T-cells represented less than 2% of the total $CD3^+$ T-cells detected (Fig. 4B); the remaining $CD3^+$ T-cells resided several hundred micrometres away from PB deposits (Fig. 4A, upper panel). Furthermore, there was no correlation between the numbers of PB deposits and $CD3^+$ T-cells in neither 12- nor 22-month-old brains (Fig. 4C). Similar results were obtained in the APP-PS1-dE9 and Tg2576 APP-tg models (data not shown). Thus, passive leucocyte extravasation was observed along with brain microhaemmorhages in aged ArcAβ mice; however microhaemorrhaging was not likely to be the main cause of T-cell invasion.

On the other hand, infiltration of T-cells could involve endothelial cell activation via expression of endothelial cell adhesion molecules. Therefore, ICAM-1 and VCAM-1 levels were investigated by immunohistochemistry in 20-24-month-old ArcAβ mice and non-tg littermate controls. Both adhesion molecules were found to be up-regulated in cortical brain areas and hippocampus of ArcAβ mice compared to non-tg controls (Fig. 4D). Examination at high magnification revealed a distinctive plaque-associated (asterisk) and vessels immunoreactivity (including large and small vessels) in ArcAβ mice (Fig. 4D inserts). Such expression was pathology-specific, as it was not observed in age-matched non-tg littermate controls (Fig. 4D) but was consistently found in amyloid-burdened brain areas of all APP-tg models examined (Supplementary Fig. 2B). Furthermore, no up-regulation of VCAM-1 and ICAM-1 was detected in the low-pathology cerebellum of the same mice (Supplementary Fig. 2A), which is also devoid of T-cell infiltration (Supplementary Fig. 1A). These results suggest that endothelial activation drives $CD3^+$ T-cell infiltration in APP-tg mice brains.

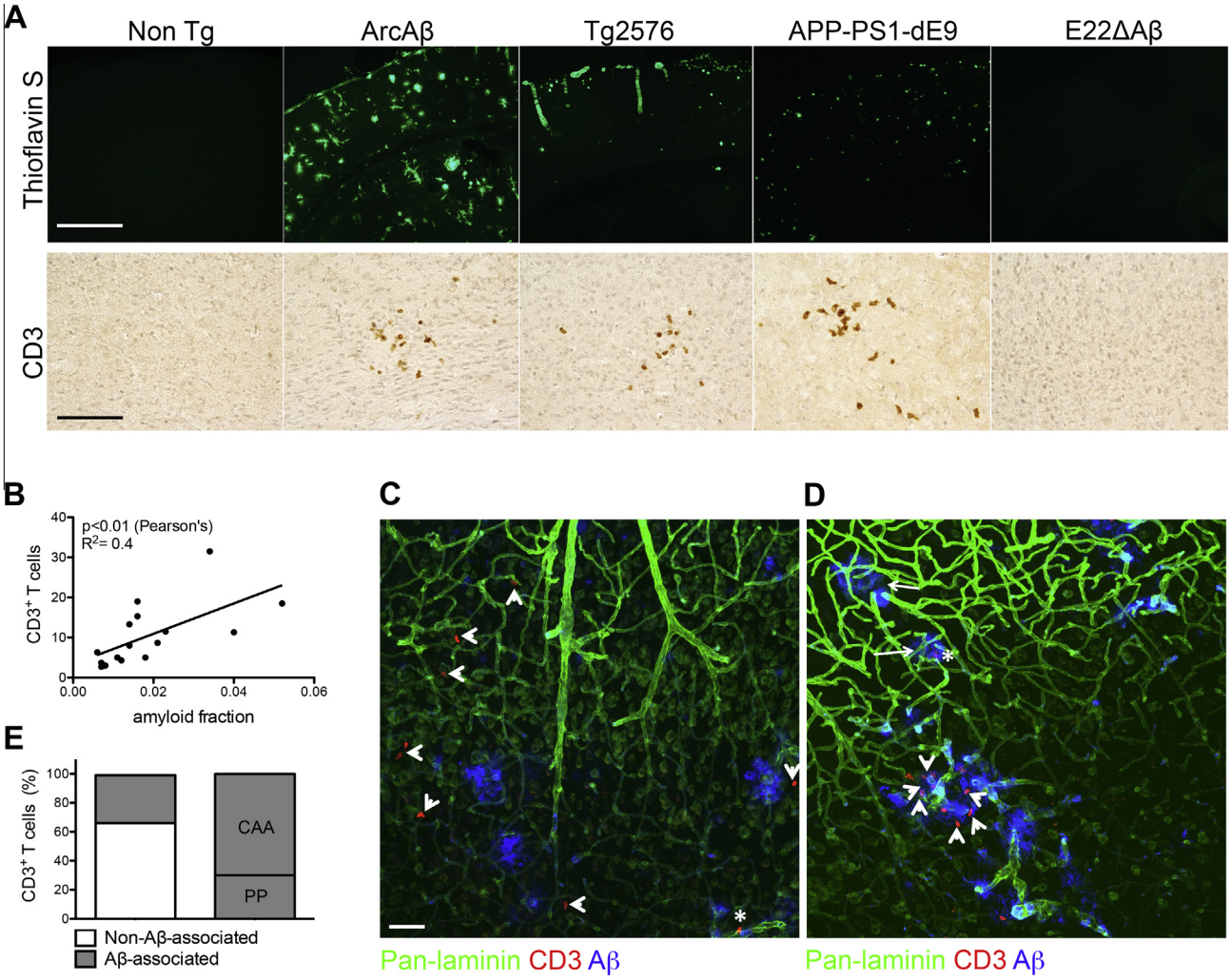

Fig. 3. Relationship between infiltrating CD3⁺ T-cells and cerebral amyloidosis. (A) Representative micrographs illustrating CD3⁺ T-cells and Thioflavin-positive amyloid deposits observed in 20–24 month old wild type and several, independent APP-tg mice. Brain parenchymal T-cells were observed in all amyloid-depositing mice models examined but not in the amyloid-free E22ΔAβ. Scale bar Thioflavin S: 300 μm, CD3: 80 μm. (B) Correlation between CD3⁺ T-cell numbers and the fractional area occupied by beta-amyloid (as detected via 6E10 antibody) in cerebral cortex and hippocampus from 15 month-old ArcAβ mice ($n = 8$, $p < 0.01$, Pearson's correlation). (C and D) Representative pan-laminin/CD3/6E10 triple-labelling in the cerebral cortex of a non-perfused 15-month-old ArcAβ mouse (images are shown as Z-stack maximal projections). Arrowheads and asterisk in (C) indicate non-Aβ-associated and a CAA-associated cell, respectively. Arrow-heads in (D) point to CAA-associated CD3⁺ T-cells, while the arrow points to a parenchymal Aβ-plaque with an associated CD3⁺ T-cells (asterisk). Scale bar = 50 μm. (E) Quantification of the frequency of non-Aβ-associated and Aβ-associated CD3⁺ T-cells in brains of 15-month-old ArcAβ. Within the Aβ-associated CD3⁺ T-cells, the proportion of CAA- versus parenchymal plaque- (PP) associated CD3⁺ T-cells is shown (average values of $n = 8$ mice examined).

3.5. CD4⁺ and CD8⁺ T-cells from ArcAβ mice show low proliferative activity and low IFN-γ expression

Having detected numerous infiltrating CD3⁺ T-cells in brains of ArcAβ mice, we asked whether these cells were proliferating locally into effector, IFN-γ-producing cells.

CD3⁺ T-cells from 12- (Fig. 5A) and 24-month-old (Fig. 5B) ArcAβ mice did not show detectable expression of the proliferation marker Ki67 via confocal microscopy, even when clustered around parenchymal amyloid plaques (Fig. 5A). The Ki67 proliferating cells observed were mostly myeloid, CD68-positive cells (data not shown). The expression levels of Ki67 were further investigated via flow-cytometry on *ex-vivo* isolated CD4⁺ and CD8⁺ T-cells from 20- to 24-month-old mice; no increase in either the frequency of Ki67-expressing cells or their fluorescence intensity in the Ki67 channel was observed in ArcAβ mice compared to non-tg littermates (Fig. 5C).

Next, we analysed via flow-cytometry the production of the effector cytokine IFN-γ by brain-derived CD4⁺ and CD8⁺ T-cells from 20 month-old ArcAβ and non-tg littermates. We observed a decreased percentage of IFN-γ producing cells in ArcAβ mice, both in the CD4⁺ and CD8⁺ T-cell subsets (Fig. 5D and E). The proportional decrease in IFN-γ-producing cells was due to an increase in the absolute numbers of the IFN-γ-negative population (Fig. 5F). Furthermore, IFN-γ expressing cells from ArcAβ mice showed lower fluorescence intensity (FI) in the IFN-γ channel, indicating lower levels of expression compared to littermate controls (Fig. 5G). The frequency and absolute numbers of CD4⁺ and CD8⁺ T-cells expressing IL-10, IL-17 and FoxP3 did not differ across the genotypes (Supplementary Fig. 5) and no significant differences in IFN-γ-producing cells were found in spleens of ArcAβ mice compared to littermate controls (Fig. 5H). Decreased frequency of IFN-γ-expressing brain-derived CD4⁺ and CD8⁺ T-cells was also observed in the APP-PS1-dE9 model of AD-like amyloidosis (Supplementary Fig. 3B). Hence, infiltrating T-cells did not proliferate locally and did not display an effector phenotype in ArcAβ brains, suggesting low activation state in the presence of cerebral amyloidosis.

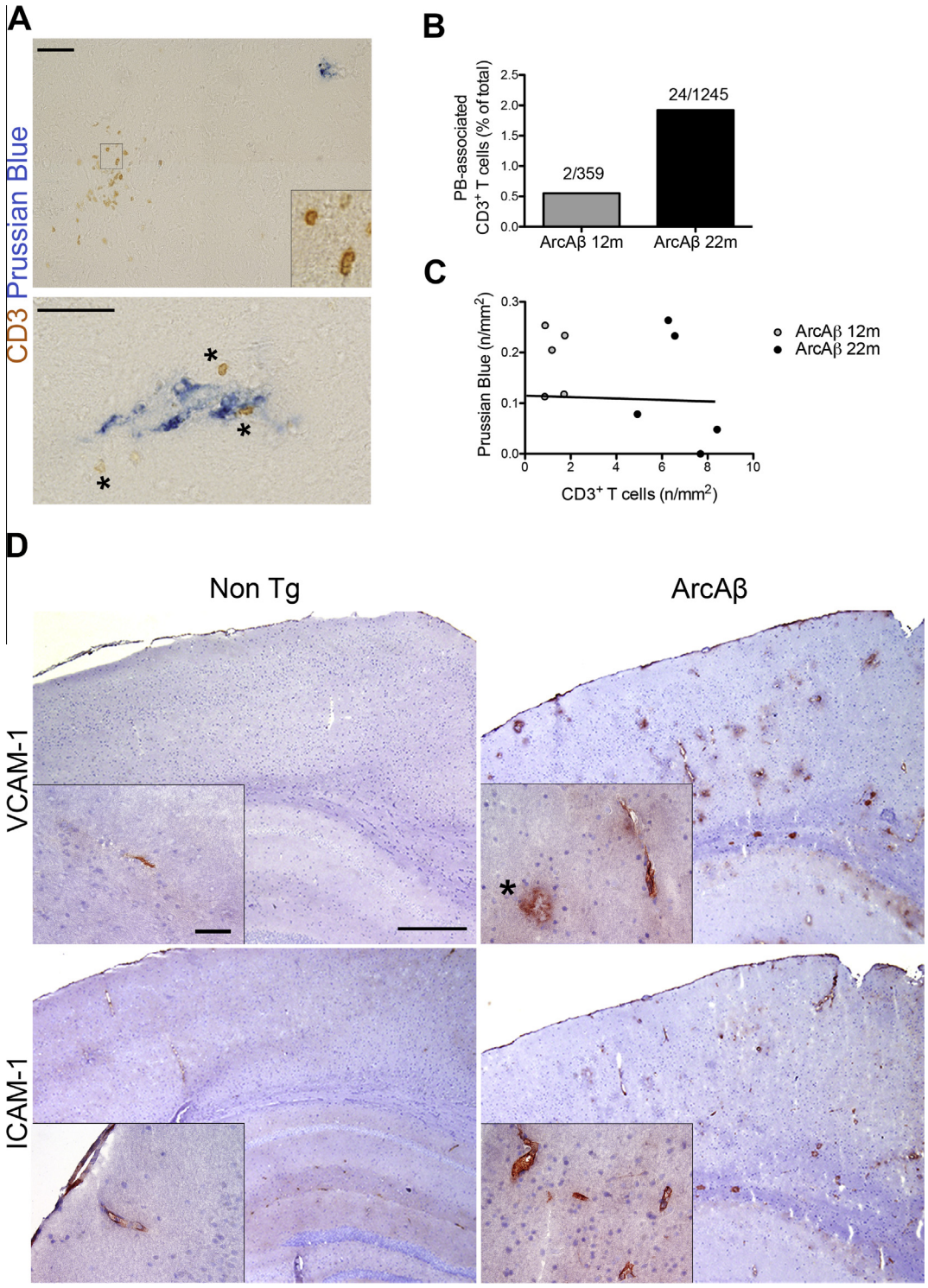

Fig. 4. Mechanisms of $CD3^+$ T-cell infiltration in ArcAβ mice brains. (A) Representative Prussian Blue (PB)/CD3 staining on a section from a 22-month-old ArcAβ mouse. The upper image illustrates the occurrence of a PB-independent cluster of $CD3^+$ T-cells in cerebral cortex (inset shows a high magnification view of the two framed $CD3^+$ T-cells). Asterisks in the lower image indicate PB-associated $CD3^+$ T-cells. Scale bar: 80 μm. (B) Percentage of Prussian Blue (PB)-associated $CD3^+$ T-cells over total $CD3^+$ T-cells detected in 12- and 22-month-old ArcAβ mice. Absolute numbers of PB-associated/total $CD3^+$ T-cells are indicated. (C) Correlation between Prussian Blue deposit and $CD3^+$ T-cell densities in brains of 12- and 22-month-old ArcAβ mice. (Spearman's correlation analysis, not significant.) (D) Representative micrographs illustrating the staining for endothelial adhesion molecules VCAM-1 and ICAM-1 in brains of 20 month-old non-tg and ArcAβ mice. Asterisk indicates typical peri-plaque staining observed in ArcAβ mice. Scale bars: 200 μm, insets: 25 μm.

3.6. Antigen-presenting cells in ArcAβ brains show an immature phenotype

T-cell activation depends on antigen-presentation by the MHC class I (MHC-I) and MHC class II (MHC-II) molecules at the surface of mature APCs, such as dendritic cells (DCs) (Banchereau and Steinman, 1998). In contrast to mature APCs, which express high surface levels of MHC-II and are potent inducers of T-cell priming and activation, immature APCs -characterised by low surface levels of MHC-II expression and accumulation of MHC-II within intracel-

lular compartments- are mostly tolerogenic (for a review: (Lutz and Schuler, 2002)). We therefore analysed MHC-II surface expression by flow-cytometry on *ex-vivo* isolated mononuclear cells derived from cerebra of 20 month-old ArcAβ and non-tg littermates (Fig. 6). Since B cells were virtually undetectable in brains of both genotypes, we focused on cells of the myeloid lineage. To distinguish resident microglia from other periphery-derived myeloid cells, we have taken advantage of their well-known differential surface expression of the markers CD45 and CD11b (Prinz et al., 2011; Greter et al., 2015). This approach allowed us to clearly identify microglial cells ($CD11b^{+}CD45^{int}$) and periphery-derived CNS "myeloid cells" ($CD11b^{+}CD45^{hi}$, e.g. perivascular and leptomeningeal DCs and macrophages, Fig. 6A). The frequency of both myeloid populations was significantly increased in the ArcAβ mice (Fig. 6A and C), with signs of microglial activation (increased expression of CD45 and CD11c, Fig. 6D and data not shown) compared to littermate controls.

We investigated the surface expression of MHC-II on microglia ($CD11b^{+}CD45^{int}$) and *bona-fide* DCs ($MHC\text{-}II^{+}CD11c^{+}CD11b^{+}CD45^{hi}$, including perivascular and letpomeningeal DCs) in our samples. $MHC\text{-}II^{+}$ microglial cells were hardly detectable in non-tg cerebra (1% of all microglial cells, Fig. 6E), and displayed only intermediate levels of MHC-II expression (Fig. 6B), in agreement with the notion of microglial cells being immature APCs (Carson et al., 1998; Aloisi et al., 2000a). In contrast, cerebrum-derived DCs, even though rare, expressed high levels of MHC-II (Fig. 6B), consistent with the known mature APCs phenotype of perivascular and letpomeningeal DCs (Colton, 2013).

ArcAβ cerebra harboured an overall increased frequency of $MHC\text{-}II^{+}$ microglial cells and DCs compared to non-tg littermates (Fig. 6E). However, the MHC-II fluorescence intensity was significantly lower in ArcAβ samples compared to controls (Fig. 6F). In fact, only the proportion of $MHC\text{-}II^{int}$ microglia and $MHC\text{-}II^{int}$ DCs was increased in ArcAβ mice samples (Fig. 6G). On the other hand, the frequency of $MHC\text{-}II^{hi}$ cells was decreased in ArcAβ samples (as in the case of microglial cells) or unchanged (in the DCs subset) compared to non-tg littermate controls (Fig. 6G). No increase in CD80 and CD86, co-stimulatory molecules required for T-cell activation, was observed in brain-derived APCs from ArcAβ samples (Supplementary Fig. 4B–D). Unchanged $MHC\text{-}II^{hi}$ cells (frequency and absolute numbers of both microglial and DCs) and increased frequency of $MHC\text{-}II^{int}$ were observed also in the APP-PS1-dE9 model of AD-like amyloidosis (Supplementary Fig. 3E–I and Supplementary Table 1). Taken together, the results suggested that APCs acquire an immature phenotype in the presence of cerebral amyloidosis.

3.7. Accumulation of intracellular MHC-II in ArcAβ brains

If APCs in ArcAβ brains display an immature phenotype, they should accumulate MHC-II in intracellular compartments. To test this, we measured total (surface plus intracellular) MHC-II expression in mononuclear cells derived from the same samples. This analysis confirmed a significant increase in MHC-II-expressing cell numbers (Fig. 6H and I). In contrast to the reduced surface expression levels (Fig. 6F) we found an unchanged expression of total MHC-II in microglia (Fig. 6J) indicating an increase in intracellular

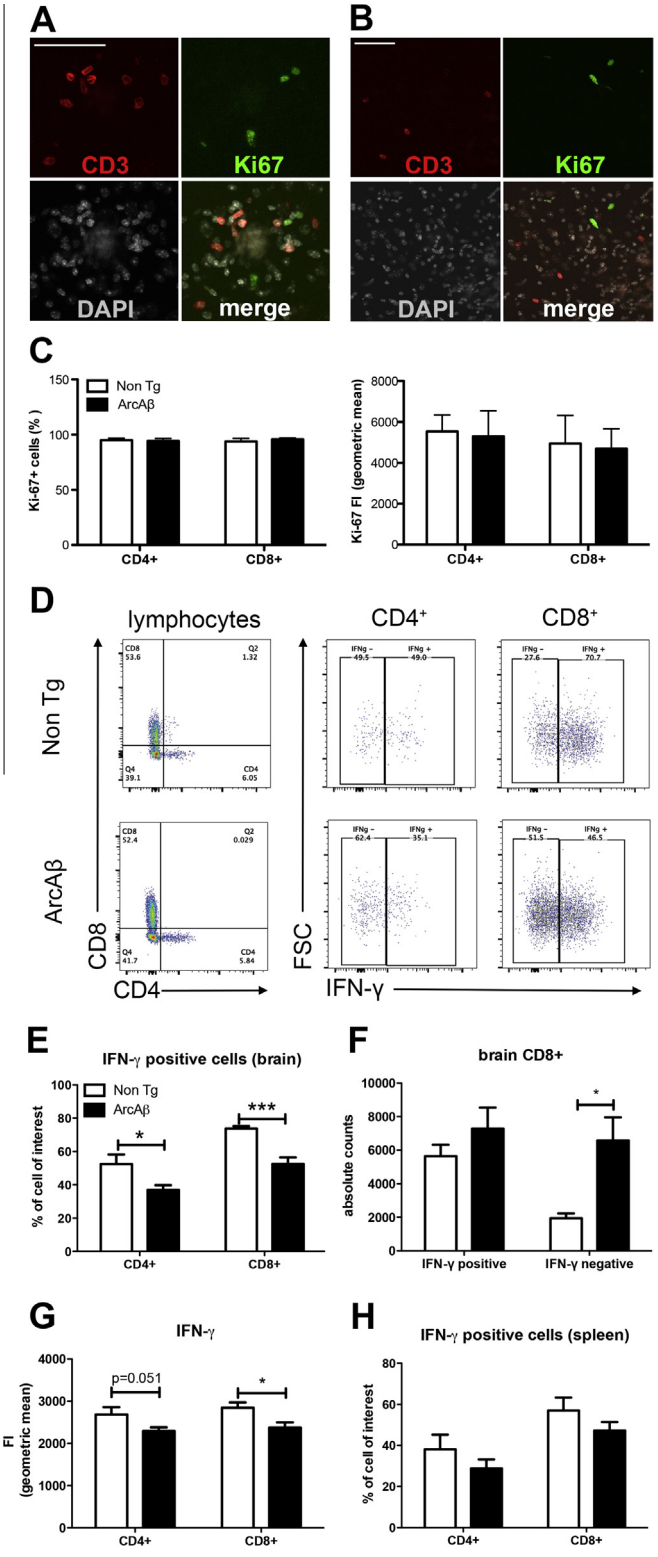

Fig. 5. Lack of proliferation and low pro-inflammatory cytokine production in brain derived T-cells from ArcAβ mice. (A and B) Representative micrographs illustrating a CD3/Ki67double staining on a 12- (A) and 24-month-old (B) ArcAβ mouse cerebral cortex. Scale bars: 50 μm. (C) Flow-cytometry analysis of Ki67 expression on CD4- and CD8-positive lymphocytes subsets from 20- to 24-month old ArcAβ mice and non-tg control littermates ($n = 4$). Data are shown as percentage as well as fluorescence intensity (FI) of Ki67 positive cells. (D) Representative dot-plots of flow-cytometry stainings of brain-derived lymphocytes from a 20-month-old ArcAβ mouse and a littermate control. Mononuclear cells were obtained from brains and stained for surface and intracellular markers of interest; $CD4^{+}$ and $CD8^{+}$ lymphocytes were gated from live $CD45^{hi}$ cells and within each compartment the expression of IFN-γ^{+} was examined. (E–G) Analysis of brain-derived $CD4^{+}$ and $CD8^{+}$ T-cells from ArcAβ mice ($n = 7$) as compared to aged-matched non-tg littermates ($n = 6$). (E) Frequency of IFN-γ^{+} cells (expressed as percentage of positive cells over total cells of interest). (F) Quantification of absolute numbers of IFN-$\gamma^{+}CD8^{+}$ and IFN-$\gamma^{-}CD8^{+}$ cells. (G) Fluorescent intensity (FI, expressed as geometric mean) of IFN-γ staining on $CD8^{+}$ and $CD4^{+}$ cells. (H) Analysis of spleen-derived $CD4^{+}$ and $CD8^{+}$ T-cell compartments. ($^{*}p < 0.05$, $^{**}p < 0.01$, $^{***}p < 0.001$, Student's *t*-test).

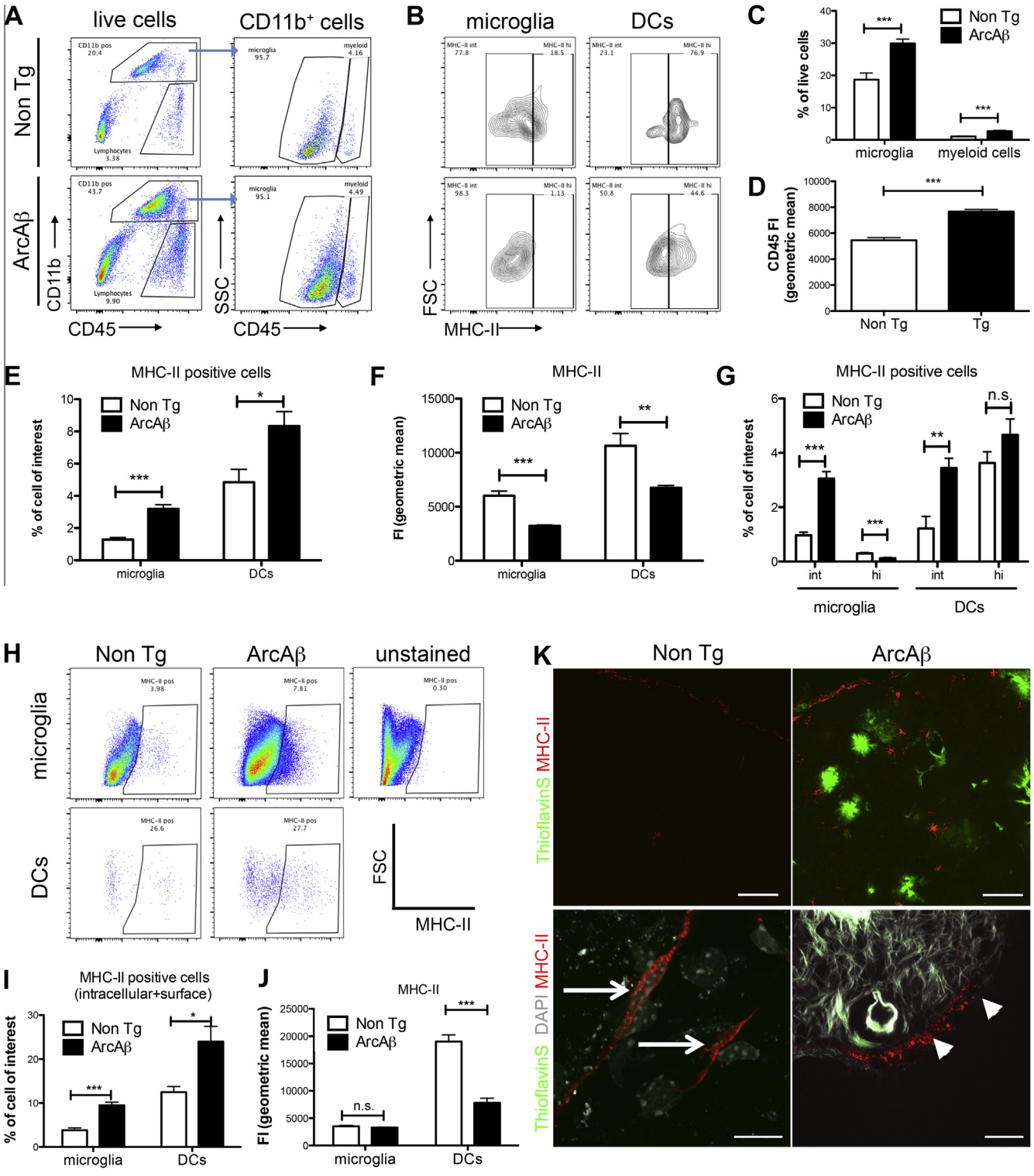

Fig. 6. Occurrence of immature APCs in cerebra of ArcAβ brains. (A) Representative dot plots of flow-cytometry surface staining of live cells from 24 month-old non-tg and ArcAβ samples. Mononuclear cells were isolated from the cerebrum and stained for markers of interest, allowing the identification of microglial cells ($CD11b^{+}$ $CD45^{int}$) and other infiltrating myeloid cells ($CD11b^{+}$ $CD45^{hi}$). (B) Analysis of MHC-II expression on $MHC\text{-}II^{+}$ microglial cells and dendritic cells (DCs: $MHC\text{-}II^{+}$ $CD11c^{+}$ $CD11b^{+}$ $CD45^{hi}$) from (A). (For details on gating see Supplementary Fig. 4A.) (C) Quantification of microglia and myeloid infiltrating cells in ArcAβ cerebrum (Tg, $n = 9$) and non-tg controls ($n = 7$). Data are expressed as frequency over live cells. (D) Fluorescence intensity (FI, expressed as geometric mean) of CD45 signal on microglial cells from A. (E–G) Quantification of $MHC\text{-}II^{+}$, $MHC\text{-}II^{int}$ and $MHC\text{-}II^{hi}$ microglia and DCs (from A and B) in ArcAβ cerebra and non-tg control littermates. (E) Percentage of $MHC\text{-}II^{+}$ cells over the cell population of interest, i.e. microglia cells or myeloid cells. (F) Geometric mean of fluorescent intensity (FI) of MHC-II signal. (G) Frequency of $MHC\text{-}II^{hi}$ and $MHC\text{-}II^{int}$ cells over the cell population of interest. (H–J) Representative dot-plot and quantification of flow-cytometry staining of total (intracellular plus surface) MHC-II on microglia and DCs. (I) Frequency of $MHC\text{-}II^{+}$ cells (expressed as percentage of positive cells over cell population of interest. (J) Fluorescence intensity (FI, expressed as geometric mean) of $MHC\text{-}II^{+}$ cells. (K) Representative MHC-II staining from the cerebral cortex of a 20-month-old ArcAβ and non-tg littermate acquired at the confocal microscopy with low (upper row, scale bar: 100 μm) and high (lower row, scale bar: 10 μm) magnification. Arrows indicate typical diffuse and membrane-bound signal on $MHC\text{-}II^{+}$ perivascular cells from non-tg brain, while arrowheads point to peculiar intracellular MHC-II immunoreactivity in a Tg sample. Data are shown as mean ± SEM. $^{*}p < 0.05$, $^{**}p < 0.01$, $^{***}p < 0.001$, Student's *t*-test. n.s. = not significant.

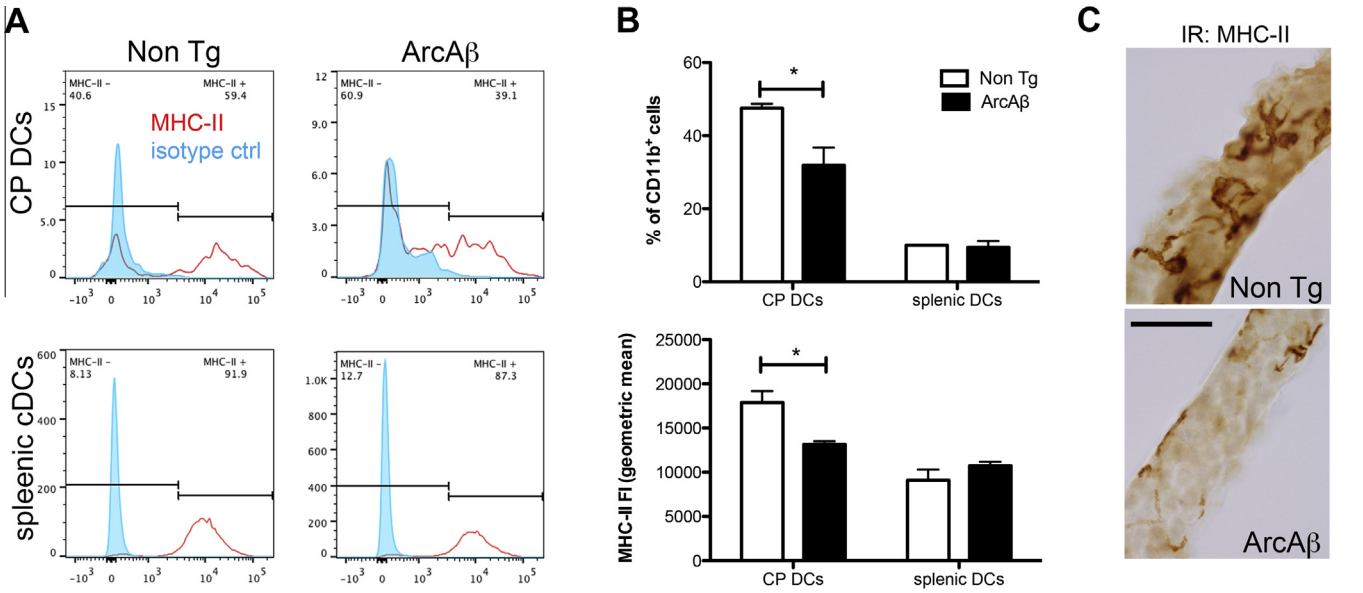

Fig. 7. Loss of MHC-II expression at the choroid plexus of aged ArcAβ mice. (A) Representative histograms of MHC-II flow-cytometry surface staining (red line) and corresponding isotype control (shaded blue) on CP-derived dendritic cells (CP DCs, $CD45^{hi}CD11b^{+}CD11c^{+}$) and splenic $CD11b^{+}CD11c^{+}$ conventional dendritic cell population (cDCs) from 24 month-old ArcAβ mice ($n = 9$) and aged-matched littermates ($n = 7$). (B) Quantification of frequency (expressed as percentage over $CD11b^{+}$ cells) and fluorescence intensity (FI, expressed as geometric mean) of the $MHC\text{-}II^{+}$ populations gated in (A). Data are shown as mean ± SEM; $^{*}p < 0.05$, $^{**}p < 0.01$, Student's *T*-test. (C) Representative MHC-II staining in the CP of an aged ArcAβ mouse and littermate control. Scale bar: 40 μm. (For interpretation of the references to colour in this figure legend, the reader is referred to the web version of this article.)

MHC-II in ArcAβ microglial cells. The accumulation of intracellular MHC-II was observed also in a second APP-tg model, the APP-PS1-dE9 (Supplementary Fig. 3J).

We next sought to confirm our flow-cytometry data using confocal microscopy. As expected, we detected several intensely labelled $MHC\text{-}II^{+}$ cells in 20-month-old ArcAβ mice brains, while only few MHC-II-positive meningeal and perivascular cells were observed in non-tg brains (Fig. 6K, upper row). When imaged at high magnification, $MHC\text{-}II^{+}$ cells from ArcAβ mice harboured a distinct and intense intracellular vesicle-like staining (Fig. 6K, lower row, arrow-heads), as opposed to the diffuse and membrane-bound signals observed in perivascular $MHC\text{-}II^{+}$ cells from non-tg brains (Fig. 6K, lower row, arrows). The vesicle-like MHC-II staining was consistent with an intracellular accumulation of MHC-II seen via flow-cytometry, and further supported the notion of an immature phenotype of APCs in ArcAβ brains.

3.8. Loss of antigen-presenting cells at the choroid plexus of ArcAβ mice

MHC-II expression was further analysed at the level of the blood–CSF-barrier in the CP, where mature DCs responsible for brain immune surveillance are known to reside (Colton, 2013; Anandasabapathy et al., 2011).

Bona-fide DCs constituted up to 40% of the $CD11b^{+}CD45^{hi}$ population, with high MHC-II-expression levels comparable to splenic DCs (Fig. 7A and B). We found that choroid plexus-DCs (CP DCs) from ArcAβ of 20-months of age were less frequent and exhibited lower MHC-II expression levels compared to age-matched non-tg littermates (Fig. 7A and B). The reduction in MHC-II expression at the CP, confirmed by immunohistochemistry (Fig. 7C), further indicated low antigen-presentation in brains of ArcAβ mice.

3.9. MHC-I up-regulation on brain-derived myeloid cells from ArcAβ mice

To complete our characterisation of brain-derived antigen presenting cells in amyloid-burdened mice, we have assessed the expression of MHC-I on brain myeloid cells via flow-cytometry and confocal microscopy. For these studies we used 22–25 month-old ArcAβ mice, since this model presented with robust infiltration of $CD8^{+}$ T-cells as of 22 months of age.

The frequency of MHC-I-positive microglia and periphery-derived myeloid cells was significantly increased in ArcAβ mice compared to aged-matched non-tg littermates (Fig. 8A and B), while it was unchanged in the amyloid-free cerebellum from the same mice (Fig. 8D). In addition, MHC-I expression was significantly up-regulated on both microglial and other myeloid cells derived from cerebrum, but not cerebellum, of ArcAβ mice (Fig. 8B and C). Confocal microscopy revealed strong MHC-I expression by perivascular Iba-1 positive cells in aged ArcAβ mice (Fig. 8C). Increased MHC-I expression at the perivascular sites might support antigen-specific recruitment of $CD8^{+}$ T-cells into the brain parenchyma of ArcAβ mice (Galea et al., 2007).

4. Discussion

There is convincing evidence from pre-clinical, epidemiological and genetic studies that the immune system plays a crucial role in AD (Wyss-Coray and Rogers, 2012; International Genomics of Alzheimer's Disease and International Genomics of Alzheimer's Disease Consortium, 2015). A decreased phagocytic activity of microglia due to chronic activation is currently regarded as the main cause of defective Aβ clearance from AD brains (Krabbe et al., 2013; Hellwig et al., 2015). Whether lymphocytes and T-cells in particular contribute to the immune dysfunction observed in AD is not known. Even though infiltrating T-cells in brains of AD patients have been consistently reported in the literature (Rogers et al., 1988; Itagaki et al., 1988; Togo et al., 2002), comprehensive examination of their localisation and activation state is lacking, probably due to the low numbers of cells of interest in the *post-mortem* brain specimens and the unsuitability of most samples for *ex vivo* flow-cytometry analysis.

On the other hand, tg mice, which reproduce severe AD-like cerebral amyloidosis, are the ideal tool to investigate the impact of amyloid on T-cell migration and function in brain. To this aim,

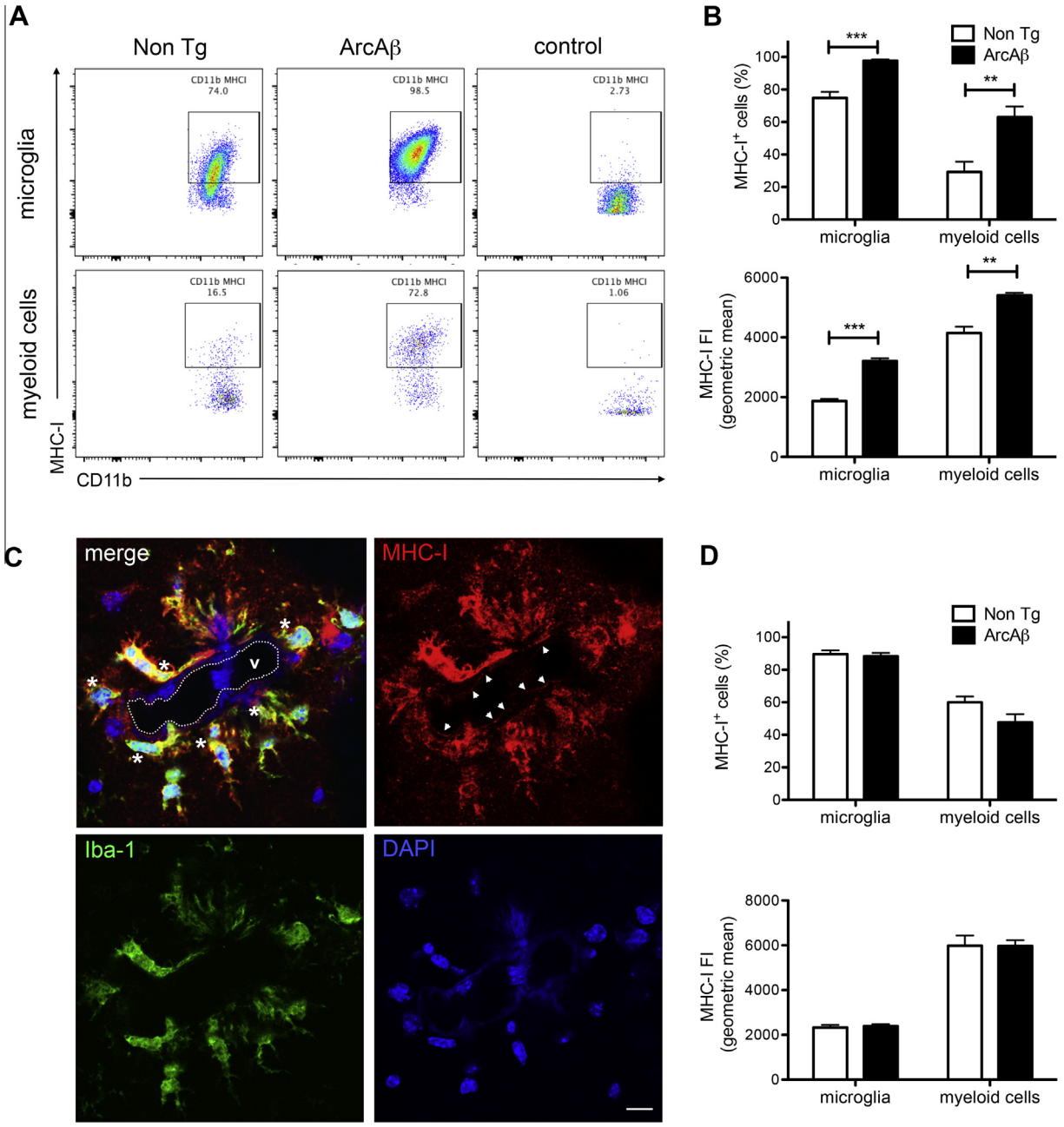

Fig. 8. MHC-I up-regulation in ArcAβ mice brain-derived myeloid cells. (A) Representative dot-plots of flow-cytometry staining of cerebrum-derived microglia and other myeloid cells from a 23-month-old ArcAβ mouse and an aged-matched non-tg littermate control. Cerebrum-derived mononuclear cells were stained for surface markers of interest; $CD11b^{+}CD45^{int}$ (microglial cells) and $CD11b^{+}CD45^{hi}$ (periphery-derived myeloid cells) were gated from live cells and examined for MHC-I expression. 'Control' illustrates the fluorescence-minus-one staining, omitting the MHC-I antibody. (B) Quantification of the MHC-I-positive cells from the cerebrum of 23–25-month old ArcAβ mice and littermate controls, as gated in (A) ($n = 4,5$). Data are shown as percentages as well as fluorescence intensity (FI) of positive cells. (C) Representative confocal images from a 22-month old ArcAβ mouse brain section double-stained with Iba-1 and MHC-I antibodies. V: outline of a vessel. Asterisks indicate perivascular Iba-1-positive cells expressing MHC-I. Arrow-heads point to MHC-I expression on the luminal surface of the endothelium. Scale-bar: 10 μm. (D) Quantification of the MHC-I-positive cells from the cerebellum of 23–25-month old ArcAβ mice and littermate controls ($n = 4,5$). Data are shown as percentages as well as fluorescence intensity (FI) of positive cells. (Data are shown as mean ± SEM. $^{**}p < 0.01$, $^{***}p < 0.001$, Student's *T*-test).

we first examined the T-cell phenotype in our in-house model, the ArcAβ mouse, which presents the advantage of harbouring abundant parenchymal plaques and CAA as of 12-months of age (Knobloch et al., 2007); subsequently, we have replicated our observations in at least one additional APP-tg model.

Indeed, all APP-tg mice depositing cerebral amyloidosis reproduced the AD-like T-cell infiltration in brain. Infiltrating T-cells were observed in amyloid-burdened areas of three APP-tg mice models, independent of background, promoter used and of APP overexpression; in fact, it was neither observed in the plaque-free E22ΔAβ mice (Fig. 3A) nor in systemic compartments (Fig. 1F). No $CD3^{+}$ T-cell was observed in RAG2-deficient APP-PS1-dE9 mice lacking mature B and T-cells, thus confirming the specificity of our technique (Supplementary Fig. 1C). The occurrence of brain infections that might explain the high $CD3^{+}$ T-cell numbers was excluded via a specific microbiological examination.

Hence, APP-tg mice are valuable models to study brain T-cells in the context of AD-like pathology. Taking advantage of APP-tg models, we have investigated the role of aging, CAA, parenchymal plaques and vascular alterations in T-cell infiltration, as well as obtained insights into their activation state.

We found that aging *per se* contributed to T-cell infiltration; in fact, brain $CD3^+$ T-cells were consistently detected in non-tg mice as of 12-months of age and were significantly increased at 22–24-compared to 12-month of age (Fig. 1A and C). However, in agreement with previous reports (Stichel and Luebbert, 2007) $CD3^+$ T-cells were observed mostly in association with nervous fibres in non-tg mice (possibly due to white matter lesions described in older individuals (Maniega et al., 2015)), while cortical areas were largely devoid of T-cell invasion. In contrast, APP-tg mice were readily distinguishable from control mice by the presence of more numerous infiltrating $CD3^+$ T-cells, localised at the grey matter of all brain cortical areas examined (Fig. 1B–D). Therefore, amyloid-dependent T-cell invasion was qualitatively and quantitatively different from the age-dependent T-cell occurrence.

Our observations in APP-tg models would support the notion that parenchymal amyloid causes brain T-cell invasion. Indeed, we found a significant correlation between $CD3^+$ T-cell numbers and amyloid fractional area in ArcAβ brains (Fig. 3B), while the cerebellum of amyloid-depositing APP-tg mice (Supplementary Fig. 1A) and the brains of E22ΔAβ mice (Fig. 3A), which are devoid of parenchymal amyloidosis, did not show invading $CD3^+$ T-cells. However, only a small fraction of infiltrating $CD3^+$ T-cells observed in 15-month old ArcAβ brains was amyloid-associated (Fig. 3C–E), similarly to previous observations (Jimenez et al., 2008). The above results suggest that cerebral amyloid is necessary but not sufficient for T-cell invasion, which is likely caused by further downstream amyloid-mediated pathological events.

APP-tg mice and ArcAβ in particular (Merlini et al., 2011) display micro bleeds and loss of BBB integrity, which could contribute to T-cell invasion. We did not observe a physical association between T-cells and micro-haemorrhages detected with PB (Fig. 4A–C). Since PB reveals residual hemosiderin that has accumulated 6 to 10 days after the occurrence of a micro bleed (Koeppen et al., 1995), T-cells might have already migrated in the parenchyma, explaining the lack of co-localisation. In this scenario, the densities of PB deposits and T-cells should correlate, even in the absence of direct spatial association. However, no such correlation was found (Fig. 4B); furthermore, no infiltrating B cells were detected (confirming (Rogers et al., 1988); data not shown), suggesting that physical BBB damage was not the cause of global lymphocyte extravasation. On the other hand, T-cell invasion in APP-tg brains was likely to be an active process relying on the interaction between endothelial adhesion molecules ICAM-1 and VCAM-1 and their cognate ligands leucocytes function-associated antigen (LFA)-1 and α4β1-integrin expressed on leucocytes (Engelhardt and Ransohoff, 2012). In fact, we observed strong up-regulation of endothelial adhesion molecules VCAM-1 and ICAM-1 in APP-tg mice brains areas, such as cerebral cortex and hippocampus, which are invaded by $CD3^+$ T-cells (Fig. 4D and Supplementary Fig. 2B), while no up-regulation was observed in cerebellum, an area spared by T-cell invasion (Supplementary Figs. 1A and 2A). Indeed increased LFA-1 ligand expression has been reported on AD brain-infiltrating T-cells (Togo et al., 2002). The cause of VCAM-1 and ICAM-1 up-regulation in amyloid-burdened areas is currently unknown; however, soluble inflammatory cytokines such as TNF, IFN-γ and IL-1β are likely to be the culprit. Such mediators, which have been shown to induce endothelial expression of both ICAM-1 (Pober, 1987) and VCAM-1 (Carlos et al., 1990), are abundantly present in amyloid-burdened brains (Heneka et al., 2015) and are highly expressed by AD-derived brain endothelial cells (Grammas and Ovase, 2001).

In addition to the VCAM-1 and ICAM-1 up-regulation, we have also observed increased levels of MHC-I at perivascular sites in the ArcAβ model. Since only activated antigen-specific $CD8^+$ T-cells are able to cross the BBB (Galea et al., 2007), this finding would support the notion that antigen-presentation at perivascular sites allows $CD8^+$ T-cells infiltration into the brain parenchyma of ArcAβ mice. Taken together, our results suggest that amyloid-induced endothelial cell activation might be responsible for T-cell infiltration in AD; further experiments are required to prove this possibility.

Infiltrating T-cells are ideally positioned to directly interact and potentially damage CNS-resident cells including neurons, astrocytes and microglia (Fig. 2D–F). Our results however do not support a cytotoxic role for T-cells in AD. Infiltrating T-cells in ArcAβ brains in fact did not actively proliferate nor displayed an effector phenotype (Fig. 5); in agreement with our results, differentiated $CD8^+$ T-cells lacking cytolytic activity have been recently described in white matter of AD and other neurological disorders (Smolders et al., 2013). The phenotype observed in APP-tg mice is rather consistent with an anergic or $FoxP3^-$ regulatory T-cell type. Regulatory or anergic T-cells, while avoiding further neuronal damage, might be limiting the beneficial activation of peripheral macrophages and microglial cells. Lack of T-cell-derived IFN-γ could impair microglia and macrophages phagocytosis (Schroder et al., 2004). Indeed, IFN-γ overexpression was shown to increase phagocytosis of Aβ-plaques and promote macrophages infiltration in naïve (Chakrabarty et al., 2010) as well as Aβ-immunized APP-tg mice (Monsonego et al., 2006); in the latter, however, clearance of Aβ-plaques came at the cost of T-cell-mediated encephalitis, suggesting that a subtle temporal and regional regulation of IFN-γ secretion is crucial for proper immune reaction in AD. Furthermore, regulatory or anergic T-cells might inhibit microglia phagocytic activity via the focal release of anti-inflammatory cytokines such as IL-10 and TGF-beta, both previously shown to modulate amyloid build-up in transgenic models (Town et al., 2008; Guillot-Sestier et al., 2015).

Supporting the possibility that the infiltrating T-cells play a regulatory role in amyloid-burdened brains, we have recently shown that RAG2-deficient APP-PS1-dE9 mice lacking mature B and T-cells display increased microglial phagocytic activity and lower Aβ burden (Spani et al., 2015). Furthermore, depletion of systemic regulatory T-cells was found to modulate microglia and promote amyloid clearance (Baruch et al., 2015). The exact mechanism of T-cell mediated microglia responses remain to be elucidated.

At the moment it is not clear what causes the low T-cell proliferation and activation state in amyloid-burdened brains. The possibility that Aβ itself directly inhibits T-cells has been previously proposed (Grant et al., 2012) and deserves further investigation. In addition, our results imply impaired antigen presentation activity in the presence of amyloidosis. Indeed, we found only few mature APCs in brain and CP samples of APP-tg mice (Fig. 6, Supplementary Fig. 3 and Supplementary Table 1) and we provided evidence for immature APCs in amyloid-burdened brains (Fig. 6, Supplementary Figs. 2 and 4). These observations are in line with previous reports indicating that exposure to Aβ induces intracellular accumulation of MHC-II in human-derived DCs (Schmitt et al., 1997) and lowers MHC-II production in murine primary microglia (Butovsky et al., 2005); on the other hand, they are at odds with the well-known up-regulation of MHC-II in AD samples (Rogers et al., 1988; Parachikova et al., 2007) and tg models (Ferretti et al., 2011). It is however possible that the up-regulation of MHC-II observed in previous studies was driven by intracellular MHC-II accumulated in immature APCs, which cannot be resolved via regular immunohistochemistry nor western blotting analysis. The lack of mature APCs in the cerebrum and CP together with the increase in immature APCs cumulatively indicates scarce antigen-presentation

capability in APP-tg brains, which might contribute to low T-cell activation. Immature APCs, in addition to their role in limiting antigen presentation, might support a detrimental inflammatory state in amyloid-burdened brains, since high intracellular levels of MHC-II have been linked to TLR-triggered immune responses via Btk activation (Liu et al., 2011).

5. Conclusions

Overall, our results suggest that amyloid deposition in brains is accompanied by low T-cell activation and down-regulation of antigen-presentation, supporting the concept of hypo-responsiveness of the immune system to Aβ (Monsonego et al., 2001). It is likely that Aβ phagocytosis is an immunological silent phenomenon (Fitzner et al., 2011), which limits the activation of the adaptive immune system to avoid detrimental autoimmunity. However, in the long term, microglial and macrophage capability to remove Aβ might decline in the absence of T cell-derived stimulatory factors and/or in response to T-cell derived inhibiting signalling. Elucidating the mechanism responsible for T-cell hypo-responsiveness and its impact on microglia function could yield novel therapeutic targets to AD.

Conflict of interest

The authors declare that they have no conflict of interest.

Acknowledgments

The Authors would like to thank Mr Daniel Schuppli and Ms Wiebke Buck for excellent technical assistance, and Dr Uwe Konietzko and Dr Rosa Paolicelli for useful discussion. M.T.F. was supported in part by the Forschungskredit grant FK-13-038 of the University of Zurich and by the Synapsis Foundation-Alzheimer Research Switzerland. T.S. was supported by the Clinical Research Priority Program Multiple Sclerosis of the University of Zurich.

Appendix A. Supplementary data

Supplementary data associated with this article can be found, in the online version, at http://dx.doi.org/10.1016/j.bbi.2016.02.009.

References

Aloisi, F., Ria, F., Adorini, L., 2000a. Regulation of T-cell responses by CNS antigen-presenting cells: different roles for microglia and astrocytes. Immunol. Today 21 (3), 141–147.
Aloisi, F., Serafini, B., Adorini, L., 2000b. Glia-T cell dialogue. J. Neuroimmunol. 107 (2), 111–117.
Anandasabapathy, N., Victora, G.D., Meredith, M., Feder, R., Dong, B., Kluger, C., et al., 2011. Flt3L controls the development of radiosensitive dendritic cells in the meninges and choroid plexus of the steady-state mouse brain. J. Exp. Med. 208 (8), 1695–1705.
Banchereau, J., Steinman, R.M., 1998. Dendritic cells and the control of immunity. Nature 392 (6673), 245–252.
Baruch, K., Rosenzweig, N., Kertser, A., Deczkowska, A., Sharif, A.M., Spinrad, A., et al., 2015. Breaking immune tolerance by targeting Foxp3(+) regulatory T cells mitigates Alzheimer's disease pathology. Nat. Commun. 6, 7967.
Butovsky, O., Talpalar, A.E., Ben-Yaakov, K., Schwartz, M., 2005. Activation of microglia by aggregated beta-amyloid or lipopolysaccharide impairs MHC-II expression and renders them cytotoxic whereas IFN-gamma and IL-4 render them protective. Mol. Cell. Neurosci. 29 (3), 381–393.
Carlos, T.M., Schwartz, B.R., Kovach, N.L., Yee, E., Rosa, M., Osborn, L., et al., 1990. Vascular cell adhesion molecule-1 mediates lymphocyte adherence to cytokine-activated cultured human endothelial cells. Blood 76 (5), 965–970.
Carson, M.J., Reilly, C.R., Sutcliffe, J.G., Lo, D., 1998. Mature microglia resemble immature antigen-presenting cells. Glia 22 (1), 72–85.
Chakrabarty, P., Ceballos-Diaz, C., Beccard, A., Janus, C., Dickson, D., Golde, T.E., et al., 2010. IFN-gamma promotes complement expression and attenuates amyloid plaque deposition in amyloid beta precursor protein transgenic mice. J. Immunol. 184 (9), 5333–5343.
Ciccarelli, O., Barkhof, F., Bodini, B., De Stefano, N., Golay, X., Nicolay, K., et al., 2014. Pathogenesis of multiple sclerosis: insights from molecular and metabolic imaging. Lancet Neurol. 13 (8), 807–822.
Colton, C.A., 2013. Immune heterogeneity in neuroinflammation: dendritic cells in the brain. J. Neuroimmune Pharmacol. 8 (1), 145–162.
Engelhardt, B., Ransohoff, R.M., 2012. Capture, crawl, cross: the T cell code to breach the blood-brain barriers. Trends Immunol. 33 (12), 579–589.
Enzmann, G., Mysiorek, C., Gorina, R., Cheng, Y.J., Ghavampour, S., Hannocks, M.J., et al., 2013. The neurovascular unit as a selective barrier to polymorphonuclear granulocyte (PMN) infiltration into the brain after ischemic injury. Acta Neuropathol. 125 (3), 395–412.
Ferretti, M.T., Bruno, M.A., Ducatenzeiler, A., Klein, W.L., Cuello, A.C., 2011. Intracellular Abeta-oligomers and early inflammation in a model of Alzheimer's disease. Neurobiol. Aging.
Fitzner, D., Schnaars, M., van Rossum, D., Krishnamoorthy, G., Dibaj, P., Bakhti, M., et al., 2011. Selective transfer of exosomes from oligodendrocytes to microglia by macropinocytosis. J. Cell Sci. 124 (Pt 3), 447–458.
Galea, I., Bernardes-Silva, M., Forse, P.A., van Rooijen, N., Liblau, R.S., Perry, V.H., 2007. An antigen-specific pathway for CD8 T cells across the blood–brain barrier. J. Exp. Med. 204 (9), 2023–2030.
Grammas, P., Ovase, R., 2001. Inflammatory factors are elevated in brain microvessels in Alzheimer's disease. Neurobiol. Aging 22 (6), 837–842.
Grant, J.L., Ghosn, E.E., Axtell, R.C., Herges, K., Kuipers, H.F., Woodling, N.S., et al., 2012. Reversal of paralysis and reduced inflammation from peripheral administration of beta-amyloid in TH1 and TH17 versions of experimental autoimmune encephalomyelitis. Sci. Transl. Med. 4 (145), 145ra05.
Greter, M., Lelios, I., Croxford, A.L., 2015. Microglia versus myeloid cell nomenclature during brain inflammation. Front. Immunol. 6, 249.
Guilliams, M., Ginhoux, F., Jakubzick, C., Naik, S.H., Onai, N., Schraml, B.U., et al., 2014. Dendritic cells, monocytes and macrophages: a unified nomenclature based on ontogeny. Nat. Rev. Immunol. 14 (8), 571–578.
Guillot-Sestier, M.V., Doty, K.R., Gate, D., Rodriguez Jr., J., Leung, B.P., Rezai-Zadeh, K., et al., 2015. Il10 deficiency rebalances innate immunity to mitigate Alzheimer-like pathology. Neuron 85 (3), 534–548.
Hellwig, S., Masuch, A., Nestel, S., Katzmarski, N., Meyer-Luehmann, M., Biber, K., 2015. Forebrain microglia from wild-type but not adult 5xFAD mice prevent amyloid-beta plaque formation in organotypic hippocampal slice cultures. Sci. Rep. 5, 14624.
Heneka, M.T., Carson, M.J., El Khoury, J., Landreth, G.E., Brosseron, F., Feinstein, D.L., et al., 2015. Neuroinflammation in Alzheimer's disease. Lancet Neurol. 14 (4), 388–405.
Hesske, L., Vincenzetti, C., Heikenwalder, M., Prinz, M., Reith, W., Fontana, A., et al., 2010. Induction of inhibitory central nervous system-derived and stimulatory blood-derived dendritic cells suggests a dual role for granulocyte-macrophage colony-stimulating factor in central nervous system inflammation. Brain 133 (Pt 6), 1637–1654.
Hsiao, K., Chapman, P., Nilsen, S., Eckman, C., Harigaya, Y., Younkin, S., et al., 1996. Correlative memory deficits, Abeta elevation, and amyloid plaques in transgenic mice. Science 274 (5284), 99–102.
International Genomics of Alzheimer's Disease C, 2015. International Genomics of Alzheimer's Disease Consortium I. Convergent genetic and expression data implicate immunity in Alzheimer's disease. Alzheimers Dement. 11 (6), 658–671.
Itagaki, S., McGeer, P.L., Akiyama, H., 1988. Presence of T-cytotoxic suppressor and leucocyte common antigen positive cells in Alzheimer's disease brain tissue. Neurosci. Lett. 91 (3), 259–264.
Jankowsky, J.L., Fadale, D.J., Anderson, J., Xu, G.M., Gonzales, V., Jenkins, N.A., et al., 2004. Mutant presenilins specifically elevate the levels of the 42 residue beta-amyloid peptide in vivo: evidence for augmentation of a 42-specific gamma secretase. Hum. Mol. Genet. 13 (2), 159–170.
Jimenez, S., Baglietto-Vargas, D., Caballero, C., Moreno-Gonzalez, I., Torres, M., Sanchez-Varo, R., et al., 2008. Inflammatory response in the hippocampus of PS1M146L/APP751SL mouse model of Alzheimer's disease: age-dependent switch in the microglial phenotype from alternative to classic. J. Neurosci. 28 (45), 11650–11661.
Knobloch, M., Konietzko, U., Krebs, D.C., Nitsch, R.M., 2007. Intracellular Abeta and cognitive deficits precede beta-amyloid deposition in transgenic arcAbeta mice. Neurobiol. Aging 28 (9), 1297–1306.
Koeppen, A.H., Dickson, A.C., McEvoy, J.A., 1995. The cellular reactions to experimental intracerebral hemorrhage. J. Neurol. Sci. 134 (Suppl.), 102–112.
Krabbe, G., Halle, A., Matyash, V., Rinnenthal, J.L., Eom, G.D., Bernhardt, U., et al., 2013. Functional impairment of microglia coincides with Beta-amyloid deposition in mice with Alzheimer-like pathology. PLoS One 8 (4), e60921.
Kulic, L., McAfoose, J., Welt, T., Tackenberg, C., Spani, C., Wirth, F., et al., 2012. Early accumulation of intracellular fibrillar oligomers and late congophilic amyloid angiopathy in mice expressing the Osaka intra-Abeta APP mutation. Transl. Psychiatry 2, e183.
Liu, X., Zhan, Z., Li, D., Xu, L., Ma, F., Zhang, P., et al., 2011. Intracellular MHC class II molecules promote TLR-triggered innate immune responses by maintaining activation of the kinase Btk. Nat. Immunol. 12 (5), 416–424.
Lutz, M.B., Schuler, G., 2002. Immature, semi-mature and fully mature dendritic cells: which signals induce tolerance or immunity? Trends Immunol. 23 (9), 445–449.
Maniega, S.M., Valdes Hernandez, M.C., Clayden, J.D., Royle, N.A., Murray, C., Morris, Z., et al., 2015. White matter hyperintensities and normal-appearing white matter integrity in the aging brain. Neurobiol. Aging 36 (2), 909–918.

Merlini, M., Meyer, E.P., Ulmann-Schuler, A., Nitsch, R.M., 2011. Vascular beta-amyloid and early astrocyte alterations impair cerebrovascular function and cerebral metabolism in transgenic arcAbeta mice. Acta Neuropathol. 122 (3), 293–311.

Monsonego, A., Maron, R., Zota, V., Selkoe, D.J., Weiner, H.L., 2001. Immune hyporesponsiveness to amyloid beta-peptide in amyloid precursor protein transgenic mice: implications for the pathogenesis and treatment of Alzheimer's disease. Proc. Natl. Acad. Sci. U. S. A. 98 (18), 10273–10278.

Monsonego, A., Imitola, J., Petrovic, S., Zota, V., Nemirovsky, A., Baron, R., et al., 2006. Abeta-induced meningoencephalitis is IFN-gamma-dependent and is associated with T cell-dependent clearance of Abeta in a mouse model of Alzheimer's disease. Proc. Natl. Acad. Sci. U. S. A. 103 (13), 5048–5053.

Ousman, S.S., Kubes, P., 2012. Immune surveillance in the central nervous system. Nat. Neurosci. 15 (8), 1096–1101.

Parachikova, A., Agadjanyan, M.G., Cribbs, D.H., Blurton-Jones, M., Perreau, V., Rogers, J., et al., 2007. Inflammatory changes parallel the early stages of Alzheimer disease. Neurobiol. Aging 28 (12), 1821–1833.

Pober, J.S., 1987. Effects of tumour necrosis factor and related cytokines on vascular endothelial cells. Ciba Found. Symp. 131, 170–184.

Prinz, M., Priller, J., Sisodia, S.S., Ransohoff, R.M., 2011. Heterogeneity of CNS myeloid cells and their roles in neurodegeneration. Nat. Neurosci. 14 (10), 1227–1235.

Ransohoff, R.M., Kivisakk, P., Kidd, G., 2003. Three or more routes for leukocyte migration into the central nervous system. Nat. Rev. Immunol. 3 (7), 569–581.

Rogers, J., Luber-Narod, J., Styren, S.D., Civin, W.H., 1988. Expression of immune system-associated antigens by cells of the human central nervous system: relationship to the pathology of Alzheimer's disease. Neurobiol. Aging 9 (4), 339–349.

Schmitt, T.L., Steger, M.M., Pavelka, M., Grubeck-Loebenstein, B., 1997. Interactions of the Alzheimer beta amyloid fragment (25–35) with peripheral blood dendritic cells. Mech. Ageing Dev. 94 (1–3), 223–232.

Schroder, K., Hertzog, P.J., Ravasi, T., Hume, D.A., 2004. Interferon-gamma: an overview of signals, mechanisms and functions. J. Leukoc. Biol. 75 (2), 163–189.

Selkoe, D.J., 2011. Alzheimer's disease. Cold Spring Harb. Perspect. Biol. 3 (7).

Shinkai, Y., Rathbun, G., Lam, K.P., Oltz, E.M., Stewart, V., Mendelsohn, M., et al., 1992. RAG-2-deficient mice lack mature lymphocytes owing to inability to initiate V(D)J rearrangement. Cell 68 (5), 855–867.

Smolders, J., Remmerswaal, E.B., Schuurman, K.G., Melief, J., van Eden, C.G., van Lier, R.A., et al., 2013. Characteristics of differentiated CD8(+) and CD4 (+) T cells present in the human brain. Acta Neuropathol. 126 (4), 525–535.

Spani, C., Suter, T., Derungs, R., Ferretti, M.T., Welt, T., Wirth, F., et al., 2015. Reduced beta-amyloid pathology in an APP transgenic mouse model of Alzheimer's disease lacking functional B and T cells. Acta Neuropathol. Commun. 3, 71.

Stichel, C.C., Luebbert, H., 2007. Inflammatory processes in the aging mouse brain: participation of dendritic cells and T-cells. Neurobiol. Aging 28 (10), 1507–1521.

Suter, T., Biollaz, G., Gatto, D., Bernasconi, L., Herren, T., Reith, W., et al., 2003. The brain as an immune privileged site: dendritic cells of the central nervous system inhibit T cell activation. Eur. J. Immunol. 33 (11), 2998–3006.

Togo, T., Akiyama, H., Iseki, E., Kondo, H., Ikeda, K., Kato, M., et al., 2002. Occurrence of T cells in the brain of Alzheimer's disease and other neurological diseases. J. Neuroimmunol. 124 (1–2), 83–92.

Town, T., 2010. Inflammation, immunity, and Alzheimer's disease. CNS Neurol. Disord.: Drug Targets 9 (2), 129–131.

Town, T., Laouar, Y., Pittenger, C., Mori, T., Szekely, C.A., Tan, J., et al., 2008. Blocking TGF-beta-Smad2/3 innate immune signaling mitigates Alzheimer-like pathology. Nat. Med. 14 (6), 681–687.

von Andrian, U.H., Mackay, C.R., 2000. T-cell function and migration. Two sides of the same coin. N. Engl. J. Med. 343 (14), 1020–1034.

Wyss-Coray, T., Rogers, J., 2012. Inflammation in Alzheimer disease-a brief review of the basic science and clinical literature. Cold Spring Harb. Perspect. Med. 2 (1), a006346.